

Electronic delocalisation in linear and cyclic porphyrin oligomers

Martin D. Peeks

Exeter College
University of Oxford

*A thesis submitted for the degree of
Doctor of Philosophy*

Michaelmas 2016

Abstract

This thesis presents a combined experimental and computational evaluation of the physical-organic properties of butadiyne-linked porphyrin oligomers. The principal result from the thesis is the synthesis and characterisation of the largest aromatic and antiaromatic systems to date, in the form of an oxidised [6]-porphyrin nanoring, with diameter 2.4 nm. This large electronically coherent system provides insight into the connection between aromatic ring currents and persistent currents in metal and semiconductor mesoscopic rings.

Chapter 1 briefly reviews the concepts used in the remainder of the thesis, with a particular focus on aromaticity.

In Chapter 2, the barrier to inter-porphyrin torsional rotation in a butadiyne-linked porphyrin dimer is determined computationally and experimentally to be 3 kJ mol^{-1} . The barrier height is closely related to the resonance delocalisation energy between the porphyrin subunits.

In ?? we show that by oxidising a butadiyne-linked [6]-porphyrin nanoring to its 4+ and 6+ oxidation states, the nanoring becomes antiaromatic and aromatic respectively. In contrast, the neutral oxidation state exhibits only local aromaticity for the six porphyrin units. The 12+ cation can also be generated, and exhibits local antiaromaticity for each porphyrin unit. The characterisation of (anti)aromaticity employs NMR and computational techniques.

In ??, the properties of cation radicals of linear and cyclic porphyrin oligomers are explored. Cations generated by spectroelectrochemistry are measured by optical spectroscopies, and chemically generated radical monocations are examined by cw/pulsed EPR spectroscopies. EPR and optical spectroscopies agree that the dimer monocation radical is fully delocalised, in Robin-Day Class III, whereas the monocations of longer oligomers are localised over 2–3 porphyrin units (Class II).

In ??, photophysical and computational investigations into excited state aromaticity in porphyrin nanorings are presented. The computational results suggest the presence of aromaticity in the triplet excited states, but experiment fails to convincingly demonstrate the effect.

Computational results in ?? show that a butadiyne linked [6]-porphyrin nanoring in which one butadiyne ($\text{C}\equiv\text{C}-\text{C}\equiv\text{C}$) is truncated to an alkyne ($\text{C}\equiv\text{C}$) exhibits a reversal of aromaticity and antiaromaticity in its oxidised states, compared to the all-butadiyne linked nanoring, consistent with Hückel's law.

Electronic delocalisation in linear and cyclic porphyrin oligomers



Martin D. Peeks
Exeter College
University of Oxford

A thesis submitted for the degree of
Doctor of Philosophy

Michaelmas 2016

*Nothing in life is to be feared, it is only to be understood.
Now is the time to understand more, so that we may
fear less.*

— Marie Skłodowska Curie, as quoted in Our Precarious Habitat (1973) by Melvin A. Benarde, p. v

Acknowledgements

Thanks everyone.

Abstract

This thesis presents a combined experimental and computational evaluation of the physical-organic properties of butadiyne-linked porphyrin oligomers. The principal result from the thesis is the synthesis and characterisation of the largest aromatic and antiaromatic systems to date, in the form of an oxidised [6]-porphyrin nanoring, with diameter 2.4 nm. This large electronically coherent system provides insight into the connection between aromatic ring currents and persistent currents in metal and semiconductor mesoscopic rings.

Chapter 1 briefly reviews the concepts used in the remainder of the thesis, with a particular focus on aromaticity.

In Chapter 2, the barrier to inter-porphyrin torsional rotation in a butadiyne-linked porphyrin dimer is determined computationally and experimentally to be 3 kJ mol⁻¹. The barrier height is closely related to the resonance delocalisation energy between the porphyrin sub-units.

In ?? we show that by oxidising a butadiyne-linked [6]-porphyrin nanoring to its 4+ and 6+ oxidation states, the nanoring becomes antiaromatic and aromatic respectively. In contrast, the neutral oxidation state exhibits only local aromaticity for the six porphyrin units. The 12+ cation can also be generated, and exhibits local antiaromaticity for each porphyrin unit. The characterisation of (anti)aromaticity employs NMR and computational techniques.

In ??, the properties of cation radicals of linear and cyclic porphyrin oligomers are explored. Cations generated by spectroelectrochemistry are measured by optical spectroscopies, and chemically generated radical monocations are examined by cw/pulsed EPR spectroscopies. EPR and optical spectroscopies agree that the dimer monocation radical is fully delocalised, in Robin-Day Class III, whereas the monocations of longer oligomers are localised over 2–3 porphyrin units (Class II).

In ??, photophysical and computational investigations into excited state aromaticity in porphyrin nanorings are presented. The computational results suggest the presence of aromaticity in the triplet excited states, but experiment fails to convincingly demonstrate the effect.

Computational results in ?? show that a butadiyne linked [6]-porphyrin nanoring in which one butadiyne ($C\equiv C-C\equiv C$) is truncated to an alkyne ($C\equiv C$) exhibits a reversal of aromaticity and antiaromaticity in its oxidised states, compared to the all-butadiyne linked nanoring, consistent with Hückel's law.

Supplement to Statement of Authorship

I did all of this except the bits I didn't.

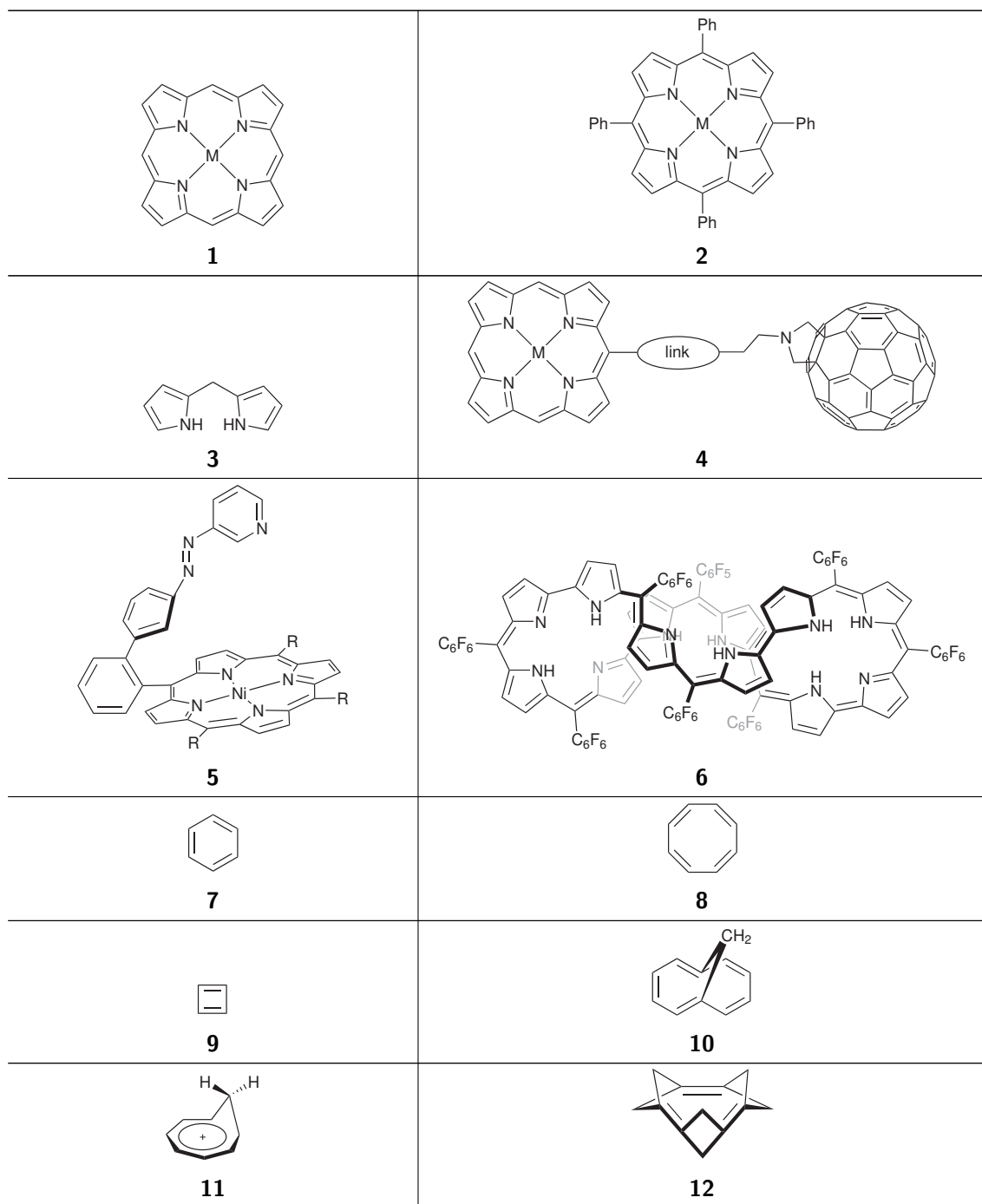
Contents

List of Publications	xi
List of Numbered Structures	xiii
1 Introduction	1
1.1 Outline	1
1.2 Porphyrins	2
1.3 Aromaticity	6
1.3.1 Early aromaticity	7
1.3.2 The aromatic sextet and Hückel's theory	8
1.3.3 Ring currents	9
1.3.4 Other experimental signs of aromaticity	12
1.3.5 Predicting aromaticity	12
1.3.6 Topological effects on aromaticity	17
1.4 The limits of electron delocalisation	20
1.5 Prospective	22
2 Experimental and computational evaluation of the barrier to torsional rotation in a butadiyne-linked porphyrin dimer	25
2.1 Abstract	26
2.2 Introduction	26
2.3 Methods	31
2.3.1 Synthesis and spectroscopy	31
2.3.2 Computational methods	31
2.4 Results and discussion	32
2.4.1 Experimental VT UV-Vis-NIR spectroscopy	32
2.4.2 Calculated electronic transitions as a function of torsion angle	34
2.4.3 Vibronic contribution to the Q-band electronic transition	37
2.4.4 van't Hoff analysis of experimental VT UV-Vis-NIR data	38
2.4.5 Evidence for enhanced conjugation in the planar conformer from C≡C bond length and vibrational frequencies	42
2.4.6 Helical molecular orbitals in twisted conformers	44
2.5 Conclusions	47
Appendices	

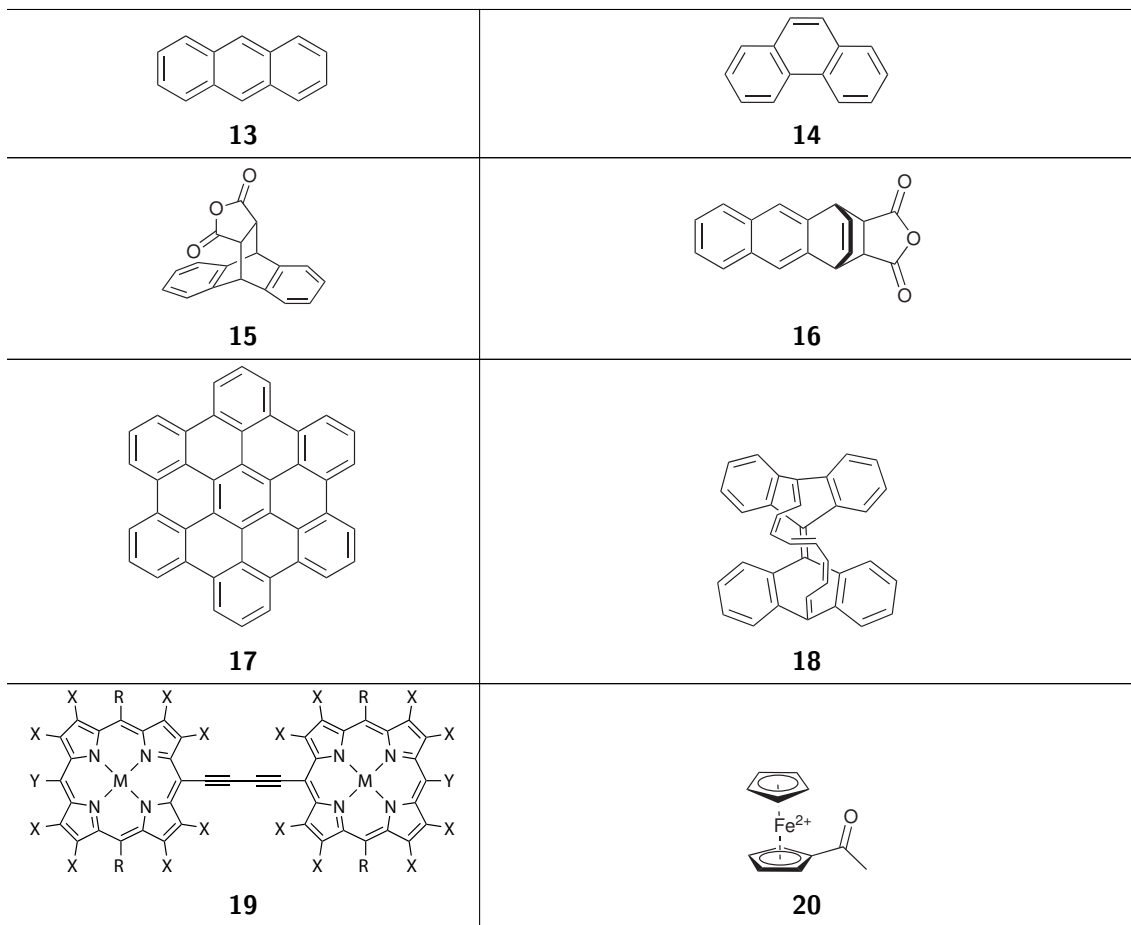
List of Publications

1. S. Richert, J. Cremers, I. Kuprov, M. D. Peeks, H. L. Anderson and C. R. Timmel, 'Constructive quantum interference in a bis-copper six-porphyrin nanoring', *Nat. Commun.*, 2017, **8**, 14842
2. M. D. Peeks, T. D. W. Claridge and H. L. Anderson, 'Aromatic and antiaromatic ring currents in a molecular nanoring', *Nature*, 2017, **541**, 200–203
3. S. Richert, M. D. Peeks, C. E. Tait, H. L. Anderson and C. R. Timmel, 'Photogenerated triplet states in supramolecular porphyrin ladder assemblies: An EPR study', *Phys. Chem. Chem. Phys.*, 2016, **18**, 24171–24175
4. G. Karunanithy, A. Cnossen, H. Müller, M. D. Peeks, N. H. Rees, T. D. W. Claridge, H. L. Anderson and A. J. Baldwin, 'Harnessing NMR relaxation interference effects to characterise supramolecular assemblies', *Chem. Comm.*, 2016, **52**, 7450–7453
5. P. Liu, Y. Hisamune, M. D. Peeks, B. Odell, J. Q. Gong, L. M. Herz and H. L. Anderson, 'Synthesis of Five-Porphyrin Nanorings by Using Ferrocene and Corannulene Templates', *Angew. Chem. Int. Ed.*, 2016, **55**, 8358–8362
6. C. E. Tait, P. Neuhaus, M. D. Peeks, H. L. Anderson and C. R. Timmel, 'Excitation wavelength-dependent EPR study on the influence of the conformation of multiporphyrin arrays on triplet state delocalization', *Phys. Chem. Chem. Phys.*, 2016, **18**, 5275–5280
7. M. D. Peeks, P. Neuhaus and H. L. Anderson, 'Experimental and Computational Evaluation of the Barrier to Torsional Rotation in a Butadiyne-Linked Porphyrin Dimer', *Phys. Chem. Chem. Phys.*, 2016, **18**, 5264–5274
8. C. E. Tait, P. Neuhaus, M. D. Peeks, H. L. Anderson and C. R. Timmel, 'Transient EPR Reveals Triplet State Delocalization in a Series of Cyclic and Linear π -Conjugated Porphyrin Oligomers', *J. Am. Chem. Soc.*, 2015, **137**, 8284–8293
9. L. D. Movsisyan, M. D. Peeks, G. M. Greetham, M. Towrie, A. L. Thompson, A. W. Parker and H. L. Anderson, 'Photophysics of Threaded sp-Carbon Chains: The Polyyne is a Sink for Singlet and Triplet Excitation', *J. Am. Chem. Soc.*, 2014, **136**, 17996–18008

List of Numbered Structures



List of Numbered Structures



List of Abbreviations

Abbreviations

2PA	Two-photon absorption
ATR	Attenuated total reflectance
bipy	4,4'-Bipyridine
BLA	Bond-length alternation
CBD	Cyclobutadiene
COT	Cyclooctatetraene
DEER	Double electron-electron resonance
DPDA	Diphenyldiacetylene
DSSC	Dye-sensitised solar cell
ECP	Effective core potential
FC	Franck-Condon
FT	Fourier transform
HBC	Hexabenzocoronene
HOMA	Harmonic oscillator model of aromaticity
HOMO	Highest occupied MO
HT	Herzberg-Teller
IR	Infra-red
IUPAC	International Union of Pure and Applied Chemistry
LUMO	Lowest unoccupied MO
MO	Molecular orbital
NIR	Near IR
NTO	Natural transition orbital
PCM	Polarisable continuum model
PDT	Photodynamic therapy
PJT	Pseudo-Jahn-Teller
ppm	Parts per million
RCM	Ring-current model
TD-DFT	Time-dependent DFT
THF	Tetrahydrofuran
UV	Ultraviolet
ZPE	Zero-point energy

Reader! Imagine a school-boy who has outgrown his clothes. Imagine the repairs made on the vestments where the enlarged frame had burst the narrow limits of its inclosure. Imagine the additions made where the projecting limbs had fairly and far emerged beyond the confines of the garment. Imagine the boy still growing, and the clothes, mended all over, now more than ever in want of mending – such is chemistry, and such its nomenclature.

— John Joseph Griffin in Chemical Recreations (7th Edition, 1834) “The Romance of Chemistry” p. 189

1

Introduction

Contents

2.1 Abstract	26
2.2 Introduction	26
2.3 Methods	31
2.3.1 Synthesis and spectroscopy	31
2.3.2 Computational methods	31
2.4 Results and discussion	32
2.4.1 Experimental VT UV-Vis-NIR spectroscopy	32
2.4.2 Calculated electronic transitions as a function of torsion angle	34
2.4.3 Vibronic contribution to the Q-band electronic transition .	37
2.4.4 van't Hoff analysis of experimental VT UV-Vis-NIR data .	38
2.4.5 Evidence for enhanced conjugation in the planar conformer from C≡C bond length and vibrational frequencies	42
2.4.6 Helical molecular orbitals in twisted conformers	44
2.5 Conclusions	47

1.1 Outline

This thesis explores electron delocalisation in porphyrin-based molecular wires, in both linear and cyclic topologies, and in neutral, cationic and excited electronic states. There is some necessity for restriction in the content of the introduction, and so only a very limited presentation of porphyrin chemistry will be made. Interested readers are referred to recent reviews,^{1–4} and to other theses from the Anderson group which deliver comprehensive introductions to porphyrin chemistry.^{5–7} The literature surrounding delocalisation of unpaired

electrons (e.g. radical cations) on conjugated oligomers and in mixed-valence compounds is mainly dealt with in ??.. For the most part, this introduction will be limited to a discussion of aromaticity, particularly in the context of organic molecules. A brief introduction to computational techniques for the assignment and prediction of aromaticity will be given.

1.2 Porphyrins

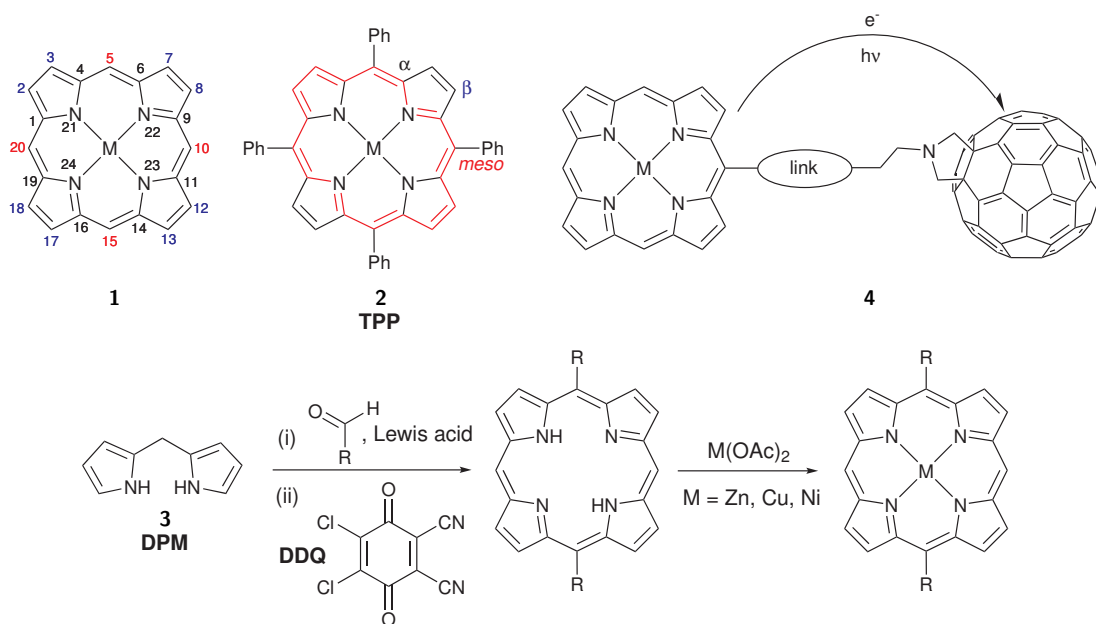
Porphyrins, with their vivid colours, have captured chemists' imaginations since the discovery of the chemical properties of chlorophyll by Willstätter, for which he was awarded the Nobel Prize in 1915.^{8,9} Chlorophyll, heme, and cytochrome proteins all contain porphyrins, and they all prove vitally important to life.

The simplest porphyrin is porphine **1** (Figure 1.1), comprising four pyrroles and four methines, arranged to form a tetrapyrrolic macrocycle with an aromatic 18 π -electron circuit. The 18 π -electron circuit can be represented by simplifying the porphyrin to an [18]-annulene (shown in red for tetraphenylporphyrin, TPP, **2** in Figure 1.1) or to a [16]-annulene dianion.^{10,11} The atomic positions of porphine can be identified by the IUPAC systematic numbering (**1**) or by the common nomenclature. In the common nomenclature the methines are referred to as the *meso* positions, the pyrrole C–Hs are referred to as the β positions, and the quaternary pyrrole carbons are the α positions, as illustrated on TPP **2**.

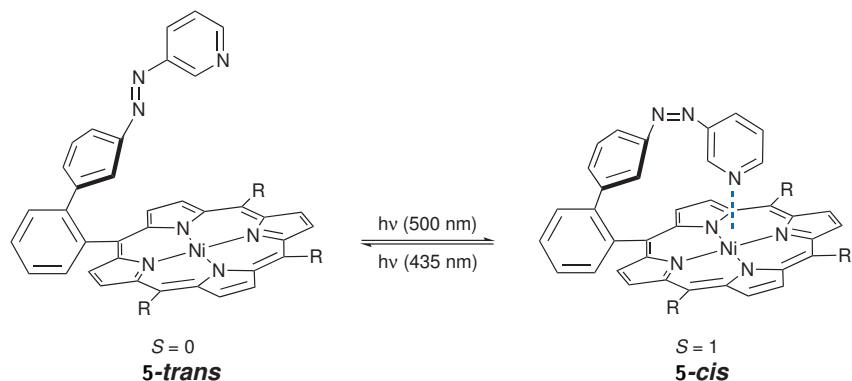
Porphyrins are typically synthesised by condensation of an aldehyde and pyrrole, perhaps via a dipyrromethane (**3**, see for example Figure 1.1).^{12,13} The resulting porphyrin monomers can be elaborated by oligomerisation, or by the introduction of substituents. In the former case, discrete porphyrin oligomers in diverse morphologies, with different linker groups, can be readily prepared (see later).^{2,3} As an example of the latter case, dyads (e.g. **4**) and triads can be prepared for exploring photoinduced charge separation.^{14,15}

The introduction of a central metal ion into a porphyrin, which acts as a square planar tetradeятate ligand, allows further modulation of the porphyrin's properties. For example, a nickel(II) porphyrin **5** has been used as a photochemical spin switch, where the action of the azobenzene photoswitch causes an axial pyridine to coordinate to the Ni(II), changing it from low spin ($S = 0$) to high spin ($S = 1$) (Figure 1.2).¹⁶ Copper(II) porphyrins are paramagnetic; they have been explored for their applications as biochemical distance rulers by double electron-electron resonance (DEER).¹⁷ Axial coordination of ligands to

1. Introduction



metalloporphyrins, yielding square pyramidal or octahedral coordination geometries, is useful for the synthesis of supramolecular assemblies (Figure 1.3), as has been recently reviewed.³



This thesis concerns the chemistry of butadiyne-linked zinc-porphyrin oligomers. This class of oligomer was first prepared by Arnold in 1978,¹⁸ and has since been the subject of intense study, mainly by his group and that of Anderson.¹⁹⁻²² Historically, Arnold focused primarily on the physical properties of short oligomers (e.g. porphyrin dimers),²⁰ whilst Anderson explored the supramolecular chemistry of porphyrins. The Anderson group has

prepared spectacular structures such as porphyrin ladders,²³ the nanoring-template complex **c-P6•T6**,²⁴ the Vernier-templated figure-of-eight **c-P12•T6₂**,²⁵ ring-in-ring complexes,²⁶ and an axially elongated nanoring tube **t-P12•T6₂** (Figure 1.3).²⁷ The preparation of these structures has relied on the binding of nitrogenous ligands – typically pyridine – to the axial coordination site of the Zn-porphyrin. The Zn-porphyrin–pyridine binding constant is weak ($K = 10^4 \text{ M}^{-1}$),²⁸ but chelate cooperativity diminishes the entropic cost for multiple-binding, leading to huge binding constants.²⁹ For example, **T6** in **c-P6•T6** has a binding constant of $K = 10^{36} \text{ M}^{-1}$.²⁴ The butadiyne link ensures good conjugation between the porphyrin units, which can readily adopt a coplanar conformation without steric hindrance, in contrast to the steric clash between porphyrin β -protons in a planar monoalkyne-linked dimer. However, as we will see in Chapter 2, there is little thermodynamic preference for planarity: the barrier to torsional rotation in a butadiyne-linked porphyrin dimer is about 2 kJ mol^{-1} .^{30,31} As such, butadiyne-linked porphyrin oligomers are prone to the introduction of conjugation-breaking defects in the form of non-planarity of adjacent porphyrin units.

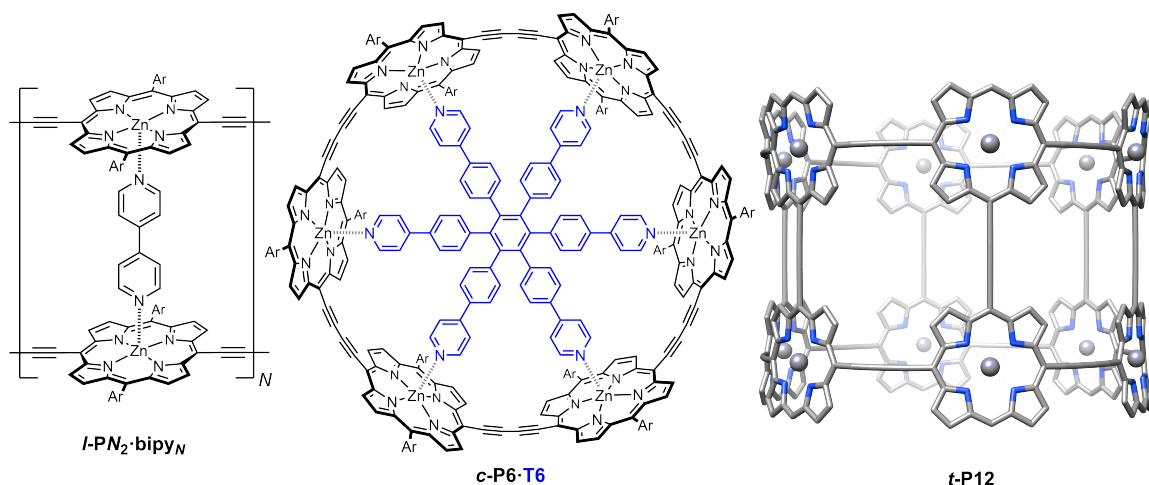


Figure 1.3: A double-stranded porphyrin ladder formed by coordination of 4,4'-bipyridine (bipy),²³ a [6]-porphyrin nanoring **c-P6•T6**,²⁴ and a [12]-porphyrin nanotube (BLYP/6-31G*) **t-P12**.²⁷

The high absorption coefficients of porphyrins and their oligomers often motivate comparisons to the light harvesting complexes in green plants, which comprise circular arrays of chlorophyll molecules.^{32,33} Efforts continue to use porphyrins in high-efficiency dye-sensitised solar cells (DSSCs), through both the design of new materials and investigations into electron transport properties.^{15,34} To date, the power conversion efficiency of synthetic DSSCs has reached 12%, compared to 22% for leading perovskite materials and 26% for

1. Introduction

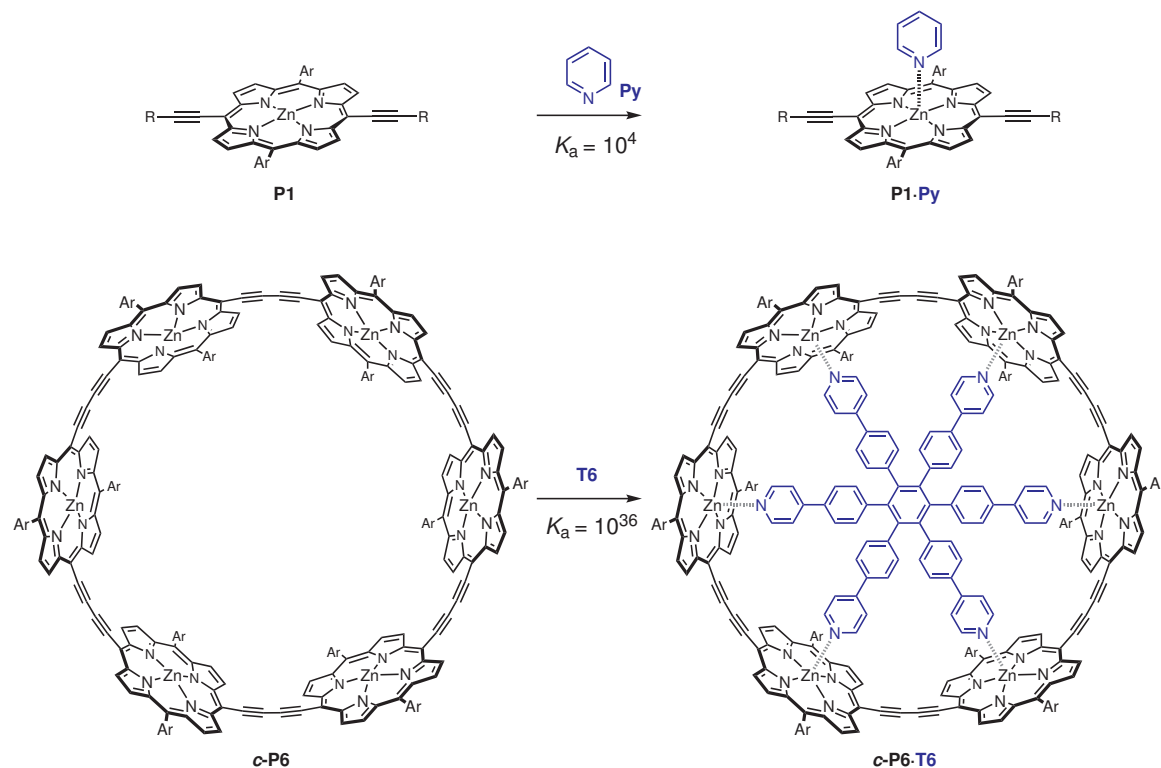


Figure 1.4: Comparison of binding constants for a porphyrin monomer to pyridine and for a [6]-porphyrin nanoring **c-P6** to a hexadentate template **T6**, demonstrating significant cooperativity in the latter.

silicon cells.³⁵ The theoretical limit for a single-junction cell, the Shockley-Queisser limit, is 34%.³⁶ Porphyrins have found more application in medicine, where they are employed for photodynamic therapy (PDT). In this treatment for cancer, a sensitiser molecule (porphyrin) accumulates in a tumour and is then irradiated with light. Intersystem crossing to the triplet manifold occurs, resulting in sensitisation of oxygen and oxidative destruction of tissue.^{37,38}

The field of porphyrin chemistry is broadened by the introduction of the porphyrinoids and the expanded and contracted porphyrins.^{39,40} These molecules are essentially variations upon the theme of the porphyrin: for example, diverse porphyrinoids can be generated by replacing the pyrroles of the macrocycle with other 5-membered aromatic rings, like furan or thiophene.^{41,42} Expanded porphyrins (e.g. **6**, Figure 1.5) are simply large porphyrinoids, with at least 17 atoms in their ‘internal ring pathway’.^{43,44} The diversity of porphyrinoids has proven extremely useful for dissecting concepts in aromaticity,^{39,45–47} including excited state and Möbius aromaticity, as we shall see in the next section.

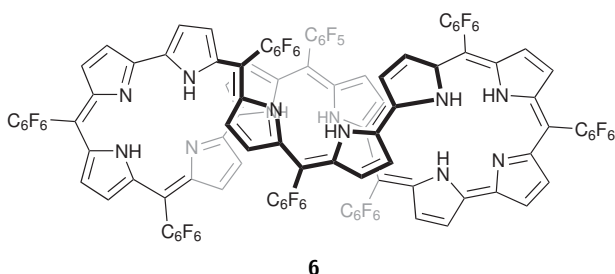


Figure 1.5: Osuka's Hückel aromatic [50]- π expanded porphyrin **6.**⁴⁸

1.3 Aromaticity

Aromaticity is a heavily-reviewed topic, and was the subject of entire issues of *Chem. Rev.* in 2001 and 2005,^{49,50} and of *Chem. Soc. Rev.* in 2015.⁵¹ In this section, a brief historical account of aromaticity will be given, illustrated by prominent examples.

A simple bibliometric analysis using Google Books⁵² shows that, although benzene was widely written about from the late 1800s, the concept of 'aromaticity' only gained prominence with the appearance of molecular orbital theory, ring current theories, and NMR (Figure 1.6a, nuclear magnetic resonance). This correlation describes the development of aromatic chemistry, from the study of compounds with particular olfactory properties to the broad-ranging subject of aromaticity, facilitated by synthetic, spectroscopic, and computational advances.

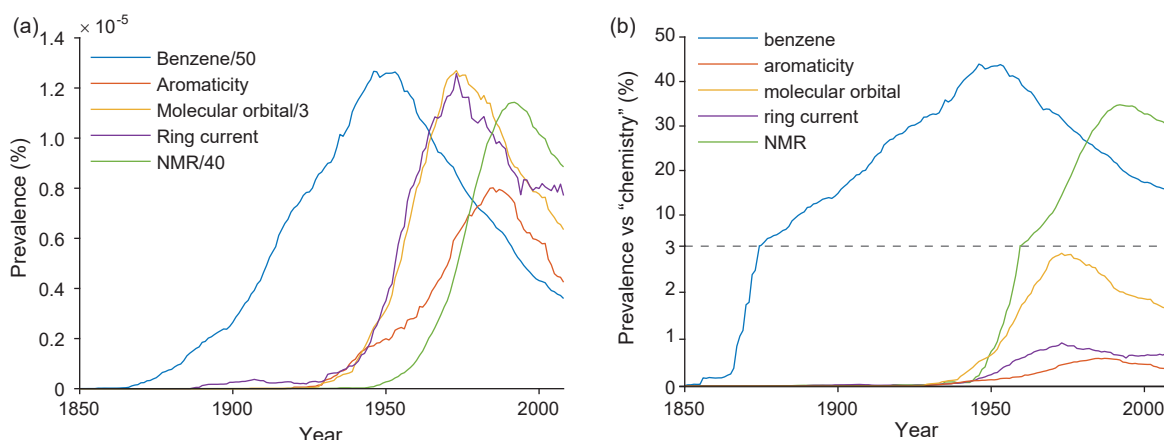


Figure 1.6: Bibliometric analysis (ngrams)⁵² showing the use of benzene, aromaticity, molecular orbital, ring current and NMR in the English language corpus of Google Books.⁵² In (a) the prevalence of each phrase, case insensitive, is shown. The numbers in the legends denote a scale factor applied to the specified term. In (b) the prevalence of the (case sensitive) terms relative to the prevalence of the word 'chemistry' are shown. All data are smoothed with a 10-point (21-year) moving average.

The decline in frequency in all of these terms since the mid-1900s is partly a consequence of chemistry forming a smaller part of the English language corpus in modern times. In

1. Introduction

Figure 1.6b, the frequencies of several terms relating to aromaticity are normalised by the frequency of the word ‘chemistry’. The results show that relative to chemistry, interest in ring currents and aromaticity has remained fairly steady since the 1980s. It is reflective of benzene’s importance that in the 1940s, the word ‘benzene’ was mentioned almost half as many times as the word ‘chemistry’!

1.3.1 Early aromaticity

Benzene (**7**, Figure 1.7) was isolated by Faraday in 1825, but its structure remained unknown until the 1860s. After Kekulé and Couper’s independent realisations that carbon is tetravalent,^{53,54} the former deduced (through the famous, perhaps apocryphal, day-dream of a snake biting its own tail) that benzene is cyclic.⁵⁵ Kekulé proposed a benzene structure with alternating single and double bonds, which he later refined by the suggestion that the single and double bonds rapidly interconverted.⁵⁶ Benzene and the other aromatic molecules became defined by reactivity, most notably by the fact that they underwent a substitution reaction with bromine, as opposed to the addition expected for alkenes (Figure 1.8).

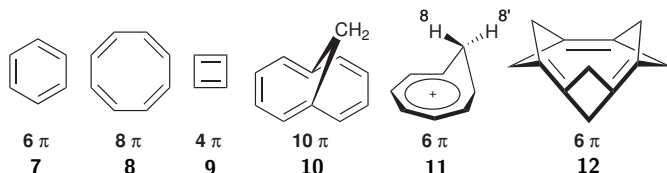


Figure 1.7: Examples of aromatic, non-aromatic, and antiaromatic compounds.

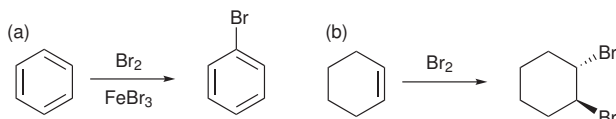


Figure 1.8: (a) Benzene undergoes a substitution reaction with bromine, in the presence of FeBr_3 as an activating Lewis Acid; (b) cyclohexene undergoes an addition reaction with benzene.

Thiele proposed a theory to account for this reactivity, namely that unsaturated carbons had a ‘partial valence’, which was especially reactive.⁵⁷ Adjacent pairs of partial valences could interact with (saturate) each other, provided neither was at a terminal position (hence, the partial valences in ethylene could not saturate). Reactivity was thus found at the unsaturated partial valences, explaining the reactivity at the 1,4-positions of 1,3-butadiene and the stability of benzene (Figure 1.9). However, Thiele’s theory was proven wrong by our earlier hero of chlorophyll chemistry, Willstätter, who isolated cyclooctatetraene

(COT, 8) in 1911,⁵⁸ and found that it reacted with bromine as an alkene, without any hint of partial valence stabilisation.

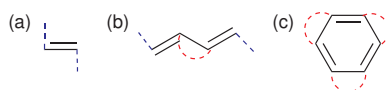


Figure 1.9: Thiele's theory of partial valences applied to (a) ethylene, (b) 1,3-butadiene and (c) benzene. Partial valences are indicated by dotted lines: blue dotted lines are unsatisfied partial valences, and thus sites of high reactivity. Saturated partial valences are denoted by red dotted semicircles: these positions are unreactive.

Although much research into aromatic compounds continued in the latter part of the 19th century, heavily motivated by their application in dyestuffs, the notion of aromaticity as a distinct chemical property did not really exist until the 1930s, with the development of molecular orbital theory, and only became ascendant as late as the 1950s (Figure 1.6).

1.3.2 The aromatic sextet and Hückel's theory

Crocker, Armit and Robinson presented the idea of the *aromatic sextet* in the 1920s, proposing that benzene's aromatic stability arose from the favourability of a sextet of valence electrons.^{59–61} Pauling and Wheland soon developed valence bond (VB) theory and the accompanying notion of resonance was quickly adopted by organic chemists. Benzene's aromatic stabilisation was explained by the presence of multiple resonance structures, in which the delocalised π -electrons are represented by different VB representations: more resonance structures confer more stability.⁶² Although Erich Hückel's molecular orbital (MO) theory was developed in the 1930s, and was able to quantitatively explain the stability of aromatic molecules, his explanations struggled to displace the pervasive and simple resonance theory.^{63,64} It was really only with the development of mnemonics, such as Doering's presentation of the $[4n + 2]$ rule⁶⁵ (bringing the theory back to aromatic sextets) and Frost and Musulin's graphical presentation of Hückel's orbital energies⁶⁶ that Hückel's MO theory entered the mainstream.⁶⁴ The familiar $[4n + 2]$ rule states that a molecule with $[4n + 2]$ conjugated π -electrons is aromatic, while a molecule with $[4n]$ π -electrons is antiaromatic, where n is a non-negative integer.

By constructing the Frost-Musulin diagrams for benzene and cyclobutadiene (CBD, antiaromatic, 9) we can immediately see that benzene, in a D_{6h} model, has a filled degenerate pair of orbitals as its highest-occupied MO (HOMO), whereas CBD, with only $[4n]$ π -electrons, adopts a triplet configuration in its D_{4h} symmetric structure (Figure 1.10).

1. Introduction

Further calculations reveal that CBD is better described as a D_{2h} rectangle, with increased double-bond and single-bond character (i.e. bond length alternation, BLA) compared to benzene.⁶⁷ This pseudo-Jahn-Teller (PJT)⁶⁸ distortion is common to the $[4n]\pi$ antiaromatic molecules, and lifts the HOMO degeneracy as shown in Figure 1.10, leading to a closed shell antiaromatic configuration with a small HOMO–LUMO (lowest unoccupied MO) gap.

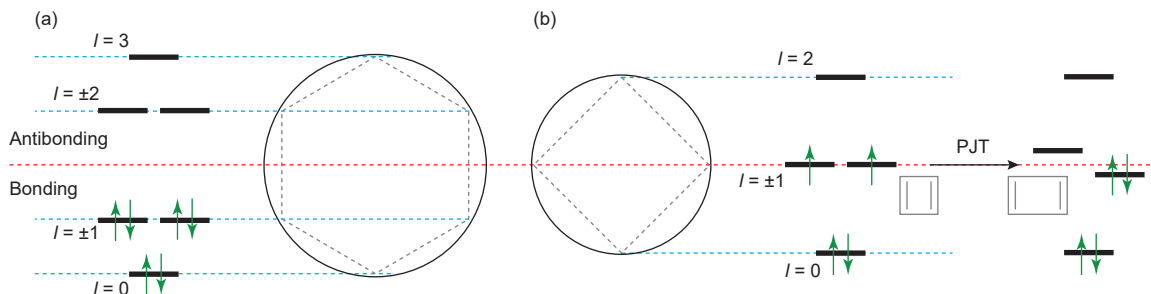


Figure 1.10: Frost-Musulin diagrams for (a) benzene and (b) CBD. In (a), all of the bonding orbitals (below the horizontal red line) of benzene are filled. In (b), the half-occupied degenerate pair is non-bonding. A pseudo-Jahn-Teller (PJT) distortion breaks the degeneracy and leads to a bonding character for one electron pair.

1.3.3 Ring currents

In addition to advances in theory, the early part of the 20th century saw a development of experimental methods for the quantification of aromaticity. Pascal noted that aromatic molecules were more diamagnetic (χ_M) than expected on the basis of additive substituent contributions (χ'_M),⁶⁹ and Pacault termed this excess of diamagnetic susceptibility the ‘exaltation’ (Λ).^{70,71}

$$\Lambda = \chi_M - \chi'_M \quad (1.1)$$

The utility of exaltation measurements for the assignment of aromaticity was demonstrated by Dauben et al. in 1969,⁷² but by this time there was a more experimentally informative, and appealing, method of measuring magnetic properties: NMR. Nowadays, susceptibility measurements have almost entirely fallen out of favour,⁷³ despite the fact that they were once described as the ‘only’ unambiguous assignor of aromaticity.⁷⁴

NMR is a particularly helpful descriptor of aromaticity because of the effect of so-called aromatic ring-currents on NMR chemical shifts. The resonances of nuclei inside an aromatic ring are shielded; those outside are deshielded. For example, the protons of

benzene are deshielded from an olefinic chemical shift (5 ppm) to what is now colloquially called ‘the aromatic region’, around 7 ppm. In the ring-current model (RCM) the delocalised π -electrons in an aromatic ring precess about the ring centre in the presence of an external magnetic field B_{ext} (typically defined along the z axis, perpendicular to the molecular plane). This precession is a *diatropic* current of electrons which flows clockwise around the ring, when viewed from the z axis (looking towards $-z$) (Figure 1.11). Consistent with Ampère’s right hand screw rule, this induced ring-current J_{ind} has an associated magnetic field B_{ind} , which opposes B_{ext} inside the ring (hence has a shielding effect) and reinforces B_{ext} outside the ring (hence deshielding). Examples of the shielding and deshielding effects arising from the RCM will be discussed shortly, but first we must give a surprisingly late introduction to antiaromaticity, via the annulenes.

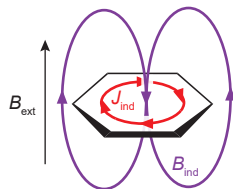


Figure 1.11: Representation of the induced ring current (J_{ind}) in benzene in the presence of an applied magnetic field (B_{ext}). The induced current generates its own magnetic field, B_{ind} which opposes B_{ext} inside the ring, and reinforces it outside.

Benzene, COT and CBD are all members of the class of molecules termed the *annulenes* by Sondheimer.⁷⁵ Annulenes are ring systems of general formula C_mH_m comprising alternating single and double C–C bonds. Sondheimer prepared a spectacular array of annulenes and dehydroannulenes, in which some C=C bonds are replaced with C≡C bonds.^{76–78} He made the remarkable discovery that while the $[4n + 2]$ -annulenes exhibited NMR spectra similar to that of benzene: i.e. shielded inner resonances and deshielded outer resonances, the $[4n]$ -annulenes had reversed spectra: inner resonances were deshielded and outer resonances shielded.⁷⁷

The term *antiaromatic* was first applied by Breslow in 1965 to describe the instability exhibited by some molecules with $[4n]$ π -electrons, antithetical to the established aromatic stabilisation of $[4n + 2]$ - π molecules.⁷⁹ In antiaromatic molecules, the ring current flows in the opposite direction (*paratropic*) to that in aromatic molecules,⁸⁰ which accounts for the opposite effects on chemical shifts.

1. Introduction

It is important to note that both aromatic and antiaromatic molecules simultaneously possess counter-rotating diatropic and paratropic ring current character to different extents. The diatropic ring current (and the diamagnetic susceptibility) is a ground state property; paratropic currents (and temperature-independent paramagnetic susceptibility) arise from interactions with excited states.⁸¹ It is easy to see why the paratropic currents can dominate for antiaromatic molecules due to the smaller HOMO-LUMO gap.

In a Hückel theory approximation, a symmetric annulene has a manifold of π -orbitals with angular momentum values $l = 0, \pm 1, \pm 2 \dots$. For aromatic molecules with $[4n + 2]$ π -electrons, these orbitals are filled to $l = \pm n$. In the antiaromatic case, the degenerate pair $l = \pm n$ is only half-filled, and can undergo distortions to lift the $l = \pm n$ degeneracy and afford a HOMO with $l = n$ and LUMO with $l = -n$. The HOMO–LUMO gap is small in this case, compared to that for an aromatic molecule (Figure 1.10), so the excited state transition (and accompanying change in angular momentum) which induces the paratropic ring currents is more accessible.^{81,82}

Fowler and Steiner have presented an alternative model in which the ring current direction is predicted by the symmetry of the dominant frontier-orbital transitions – in this model, both diatropic and paratropic ring currents arise from transitions to excited states. A rotationally allowed transition (as between a Jahn-Teller distorted angular-momentum pair) leads to a paratropic current, while a translationally allowed transition (as between $l = \pm n$ and $l = \pm [n + 1]$) leads to diatropicity.^{80,83} More thorough introductions to the quantum mechanical origin of ring currents and magnetic susceptibilities can be found in the cited reviews and references therein.^{84,85}

The NMR shielding effect inside an aromatic ring can be probed by molecules where an NMR-active nucleus is located inside the ring. Vogel and coworkers were able to synthesise a [10]-annulene derivative with a methylene bridge above the annulene plane (1,6-methanocyclodecapentaene, **10**): as expected from the RCM, this methylene is shielded by about 2–3 ppm to -0.5 ppm.⁸⁶ The propensity of Li^+ to coordinate to the π -systems of aromatic molecules can also be exploited, allowing the use of ${}^7\text{Li}$ NMR to measure the ring-current shielding effect.⁷⁴

Porphyrin chemistry provides many examples of the ring current shielding effects for aromatic and antiaromatic derivatives. The porphine ligand is formally in a 2– oxidation

state with an aromatic set of 18 π -electrons. Typically, a 2+ metal binds to the porphyrin to give a net zero charge, as is the case for M = Zn, Mg, Ni, 2H, etc. In the latter case, M = 2H, the protons are characteristically shielded from a pyrrolic 8 ppm to -2 ppm. Vaid and coworkers have prepared a TPP complex of Si, where the TPP ligand has a -4 (20π) oxidation state. ^{29}Si NMR shows that the central Si is deshielded by 125 ppm on account of the antiaromatic ring-current.⁸⁷

1.3.4 Other experimental signs of aromaticity

There are other properties available by which to assign aromaticity. The most traditional of these is based on aromatic reactivity: a propensity to undergo electrophilic aromatic substitution rather than addition. A related aspect is the energetic stability of aromatic systems, arising from a large resonance stabilisation energy (contrast to zero, or negative, stabilisation for antiaromatic systems). Finally, structural properties can support an assignment of aromaticity: aromatic compounds exhibit a low BLA, whereas the pseudo-Jahn-Teller distortion for antiaromatic compounds leads to a higher BLA. Such data can come from infra-red (IR) or Raman spectroscopies, X-ray diffraction, or from calculation.

1.3.5 Predicting aromaticity

There is a multitude of methods available to computationally predict and characterise aromaticity in molecules. Their utility is facilitated by the availability of computing power and the applicability of density functional theory (DFT), which scales well for small molecules (systems with a few hundred atoms are routine) with generally accurate results.

1.3.5.1 Ring currents

Perhaps the most popular methods for predicting aromaticity are those which measure the properties of the aromatic ring current. The first of these techniques was the nucleus independent chemical shift (NICS), which evaluates the NMR shielding at a point in space around a molecule. This is achieved by placing a ‘ghost’ atom (in Gaussian, ‘Bq’, after the character (latterly a ghost) Banquo⁸⁸ in *Macbeth*) at the desired probe position(s). In the first reported NICS calculations, the ghost atoms were placed at the geometric centres of rings.⁸⁹ For some inorganic ring systems, it was noted that the in-plane NICS was prone to contamination by σ and in-plane π bonds, motivating the dissection of π and σ components

1. Introduction

to give NICS_π and NICS_σ .⁹⁰ The measurement of $\text{NICS}(X)$ at some position $X \text{ \AA}$ above the ring plane was also used for these inorganic systems, to avoid in-plane contributions.⁹⁰ Indeed, it had been earlier noted that NICS values were higher above the ring plane than in the plane for small π -aromatic systems, reflecting the toroidal distribution of π -electrons and the presence of σ bond anisotropy contamination for in-plane measurements.⁸⁹

In addition to choosing a suitable z -axis height, the selection of the correct tensor component to describe aromaticity is also important: the original report used the isotropic (iso) shielding (NICS_{iso}),⁸⁹ but later studies have placed increased emphasis on the zz shielding tensor component (NICS_{zz}) as being more reflective of aromaticity effects. Of the myriad combinations of ‘dissected NICS’ (i.e. π contributions only), distances above the ring plane, and tensor components, it was found that $\text{NICS}(0)_{\pi zz}$ gave the best correlation to aromatic stabilisation energy, and that the non-dissected $\text{NICS}(1)_{zz}$ was a suitable alternative, since shifting the ghost atom 1 \AA above the ring plane has the effect of removing most in-plane contamination.

Since its invention in the late 1990s the NICS method has been extended to the calculation of shielding isosurfaces⁹¹ and NICS-scans⁹² which reveal the variation in aromaticity in different parts of a molecule.^{92,93} Examples of the utility of NICS and its derivatives have been thoroughly reviewed.^{73,94}

NICS evaluates the effects of the ring current: the magnetic shielding and deshielding. It is also possible to computationally predict and visualise the ring current. The anisotropy of the induced current density (ACID) method depicts the induced current as an isosurface around the molecule.⁹⁵ By examining this anisotropy property, rather than just the current density field, it is possible to subtract out local diamagnetic (isotropic) atomic ring currents, which otherwise dominate. As a result, electron delocalisation can be visualised as a three-dimensional isosurface around the molecule (Figure 1.12).

ACID was first applied by Wallenborn et al. to assess transition state aromaticity,⁹⁶ and the utility of the technique was significantly broadened from aromaticity to other examples of conjugation, including hyperconjugation and spiroconjugation, by Herges et al.^{95,97} An illustrative example of ACID’s application to porphyrin ring currents shows the utility of the technique in dissecting electron delocalisation pathways.⁴⁶ The additional calculation of induced current vectors shows the direction of electron flow in the presence of an applied field, and thus the assignment of diatropic and paratropic ring currents.⁹⁷

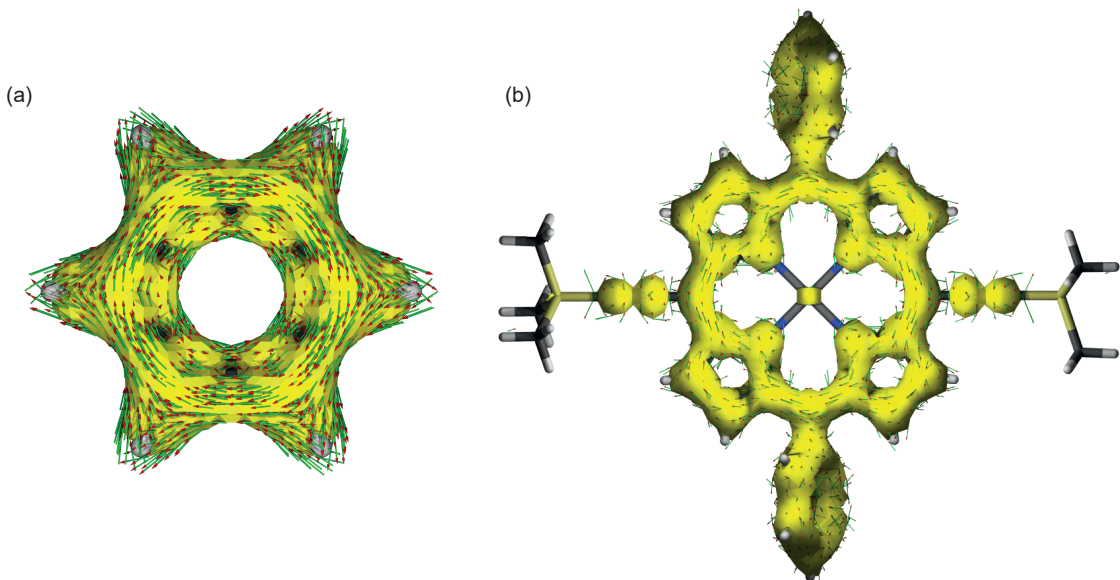


Figure 1.12: ACID isosurfaces (yellow, isovalue = 0.05) and current vectors (green/red) for (a) benzene and (b) a zinc porphyrin monomer. The monomer is substituted with trimethylsilylacetyles. B3LYP/6-31G* (LANL2DZ ECP for Zn). The current vectors are calculated for an applied magnetic field perpendicular to the aromatic ring planes (i.e. out of the page).

It is also possible to directly calculate the magnitude of the ring current passing through a given bond. The Gauge-Including Magnetically Induced Currents (GIMIC) technique is popular for this calculation, and several examples of its use have been reported.^{98–100}

1.3.5.2 Structural

In benzene, all of the C–C bonds are of equal length: there is no BLA, indicating complete electron delocalisation. The extent of BLA in a molecule can be quantified using the harmonic oscillator model of aromaticity (HOMA)¹⁰¹

$$\text{HOMA} = 1 - \left[\frac{\alpha}{N} \sum_i^N (R_{\text{opt}} - R_i)^2 \right] \quad (1.2)$$

$$= 1 - \alpha(R_{\text{opt}} - R_{\text{av}})^2 - \frac{\alpha}{N} \sum_i^N (R_{\text{av}} - R_i)^2 \quad (1.3)$$

$$= 1 - \text{EN} - \text{GEO} \quad (1.4)$$

where HOMA is a quantity from 0 (complete localisation) to 1 (complete delocalisation), α is an empirical scaling constant, N is the number of bonds over which the sums run, R_i is the length of the i^{th} bond, R_{av} is the average bond length, and R_{opt} is the optimum bond length for a fully delocalised bond (e.g. 1.388 Å for C–C).¹⁰¹ In other words, the first term

1. Introduction

(EN) relates to an increase (vs. the optimum) in mean bond length in the system, and the second term (GEO) relates to the amount of BLA. Both of these parameters indicate non-aromaticity, and hence a decrease in HOMA towards zero.¹⁰²

The theory and application of structural descriptors of aromaticity have been reviewed by Krysowski and Cyrański.¹⁰³ Although BLA is a good metric for aromaticity in small molecules, it has been shown computationally that [30]-annulene exhibits the magnetic characteristics of aromaticity despite the presence of significant BLA, and even larger annulenes (up to [66]-annulene) are aromatic if high symmetry (D_{6h}) is retained.^{104,105}

1.3.5.3 Energetic

The increased thermodynamic stability conferred by aromaticity is often termed the aromatic stabilisation energy (ASE), and can be calculated explicitly. The forerunners of the ASE methods were estimations of resonance energy, either by experiment or calculation.^{71,106}

In calculations of resonance energy, the additional stabilisation of aromaticity is taken as the difference between the aromatic molecule's energy and the energies of the substituent 'localised' components. For example, the resonance energy of benzene can be estimated by the difference of benzene's electron energy and the sum of its bond contributions: three C=C, three C–C and six C–H. These approaches require the energy of the aromatic molecule, and reliable energies for the localised substituents.

The calculation of ASE depends on devising, and calculating, a suitable reaction scheme which directly reports on the aromaticity of the molecule, whilst avoiding contributions to the reaction energy from changes in hybridisation or atom numbers. The two primary methods are the homodesmotic stabilisation energy (HSE) and its improved form: the isomerisation stabilisation energy (ISE) (Figure 1.13).¹⁰⁷ In the former, starting materials and products have the same number of atoms with the same hybridisation. In the latter, the aromatic molecule is optimised with a methyl substituent: the ISE comes from the difference in energy when the methyl is converted into an exocyclic double bond with accompanying loss of aromaticity.

The ISE has been evaluated for the annulenes from benzene ([6]-annulene) to [66]-annulene (Figure 1.14).¹⁰⁴ As ring size increases, ISE-per-electron becomes vanishingly small: for example, [42]-annulene has an ISE-per-electron of 2.3 kJ mol⁻¹. Put into context, this is about the same as the entropic cost, at room temperature, of freezing a sp²–sp² torsion.¹⁰⁸ This comparison implies that, for large annulenes, the aromatic stabilisation

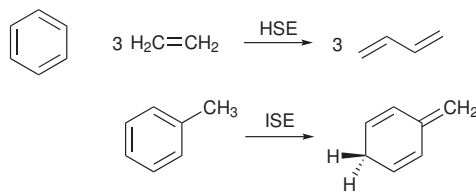


Figure 1.13: (top) A homodesmotic reaction for calculating the HSE of benzene; (bottom) the reaction scheme for calculating the ISE of benzene.

energy becomes vanishingly small compared to the entropic cost of maintaining a regular cyclic geometry necessary for aromaticity.

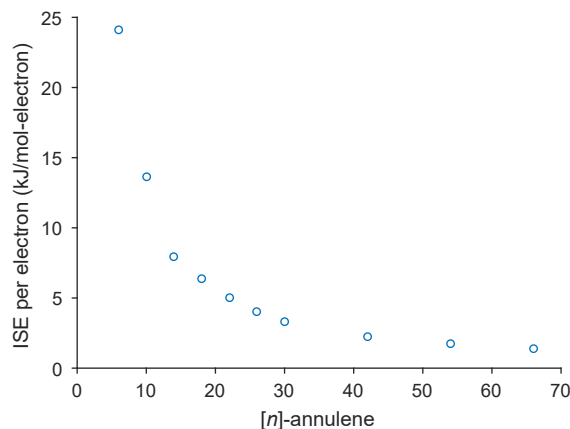


Figure 1.14: Isomerisation stabilisation energy (ISE) per electron for the annulenes, B3LYP/6-31G*. Data from Wannere and Schleyer.¹⁰⁴

1.3.5.4 Electronic

There has been a recent adoption of computational aromaticity metrics which describe electron delocalisation directly, rather than a physical observable such as BLA, or magnetic properties. These metrics have recently been reviewed.¹⁰⁹ Indeed, the ACID method (see Section 1.3.5.1) also falls into this category. Without going into too much detail, many electron-delocalisation measures are calculated by evaluating the nature of the electron density at bond critical points and ring critical points (i.e. at the centres of bonds and rings), within the framework of the Quantum Theory of Atoms in Molecules.¹¹⁰ In contrast to the other methods presented above, wavefunction analysis is perhaps the most remote from an experimental observable (cf. NMR for NICS, crystallography for structural properties, and calorimetry for stabilisation energies).

1. Introduction

1.3.6 Topological effects on aromaticity

The annulenes are all monocyclic carbocycles, but molecules can exhibit much broader topological diversity, which has implications for the assignment of aromaticity. In this section we discuss, roughly in order of their appearance in the literature, polycyclic aromaticity and Clar's rule, homoaromaticity, and Möbius aromaticity.

1.3.6.1 Polycyclic aromaticity

Some of the earliest identified aromatic compounds, on the basis of smell, were those comprising fused benzene rings. These molecules exhibit some non-aromatic character in their reactivity: anthracene (**13**), comprising three linearly fused benzene rings, undergoes Diels-Alder reaction at the 9,10-positions of the central benzene ring. Phenanthrene (**14**) has distinctly olefinic chemistry at its 9,10-positions. These observations were rationalised by Clar, who noted that the aromaticity of a polybenzenoid molecule depends on the number, and location, of discrete aromatic sextets of six π -electrons.¹¹¹ In anthracene, three resonance structures, each with one sextet, can be drawn; Diels-Alder chemistry at the 9,10-positions offers a product with two Clar sextets (**15**), while reaction at either of the terminal benzene rings gives just one Clar sextet (**16**). Hence reactivity is exclusively at the 9,10-positions. For phenanthrene (**14**), the maximum possible number of sextets is two, for the terminal rings, leaving olefinic character in the central ring (Figure 1.15).¹¹²

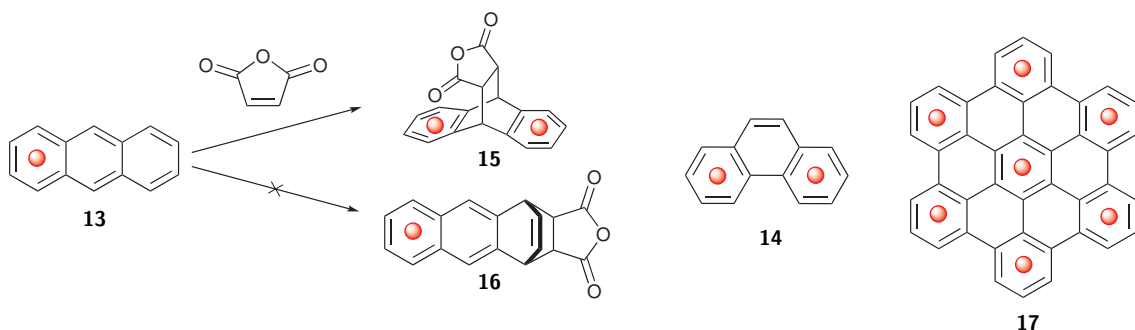


Figure 1.15: Examples of polycyclic aromatic hydrocarbons, and the application of Clar's rule to predict and rationalise aromatic character. The red dots denote aromatic sextets.

This idea has been extended to hexabenzocoronene (HBC), which has a maximum of seven aromatic sextets. Spectacularly, the different aromatic and single bond character predicted by Clar's rule is measurable by atomic force microscopy (AFM).¹¹³

Porphyrins present another example of polycyclic aromaticity: they essentially comprise an [18]-annulene $[4n + 2]$ π -electron pathway appended by two (spectator) ethylene bridges and two aromatic 6 π -electron pyrroles. Both of these aromatic ring current paths are important to the porphyrin aromaticity, though on an atom-weighted basis the pyrroles contribute more aromatic stabilisation energy.⁴⁶ The aromatic stabilisation energy (ASE) calculated by the block-localised wavefunction method to isolate the π -electron effects shows that the ASE from the macrocyclic [18] π -electron circuit in the porphyrin is the same as that of an individual 6 π -electron pyrrole ($\sim 80 \text{ kJ mol}^{-1}$).⁴⁶

1.3.6.2 Homoaromaticity

The homoaromatics comprise a different sort of topological perturbation of the monocyclic π -framework of the annulenes: introduction of an insulating (e.g. CH₂) interruption. Remarkably, aromaticity and conjugation can persist in charged species despite this disruption. So, the homotropylium cation **11** (C₈H₉⁺, Figure 1.7) is distinctly aromatic, as revealed by the different chemical shifts of protons 8 (inside, -0.6 ppm) and 8' (outside, 5.2 ppm).^{71,114}

Homoaromaticity is much rarer for neutral species,⁷¹ and seems to arise only when the π -orbitals on either side of the conjugation defect are close enough to effect delocalisation, such as in the theoretical trishomoaromatic molecule **12** (Figure 1.7).¹¹⁵

1.3.6.3 Möbius aromaticity

Heilbronner (1964) predicted that the introduction of a 180° phase shift into the aromatic π -system would reverse Hückel's law: such a molecule with $[4n]$ π -electrons is then aromatic, and $[4n + 2]$ π -electrons becomes antiaromatic.¹¹⁶ Such molecules are known as Möbius aromatic molecules, for their resemblance to the topological Möbius strip (Figure 1.16).

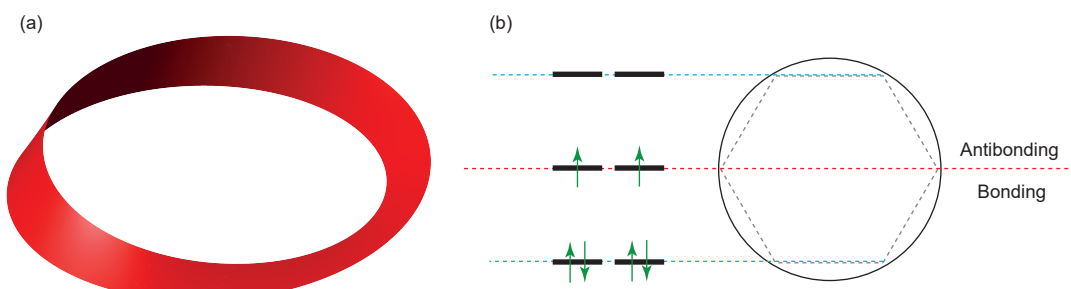
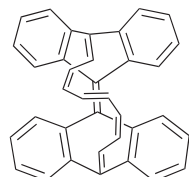


Figure 1.16: (a) A Möbius strip. (b) A Frost-Musulin diagram for a hypothetical 6 π -electron Möbius molecule.

1. Introduction

The first synthetic example of a Möbius aromatic molecule was given by Herges and coworkers: the twisted [16]-annulene **18** (Figure 1.17) is aromatic.¹¹⁷ It is possible to introduce two Möbius twists into a molecule, at which point it reverts back to Hückel's aromaticity rules.^{118,119} Several examples of expanded porphyrins which exhibit Möbius aromaticity have been reported by Osuka and co-workers.¹²⁰



18

Figure 1.17: Example of Möbius aromatic compound **18**.¹¹⁷

1.3.6.4 Excited state aromaticity

In molecules which exhibit excited state (anti)aromaticity (ES(A)A), the electron-counting rules are once again reversed (Table 1.1).^{121,122} The effect has been reported in expanded porphyrins by Osuka and co-workers, and was assigned on the basis of the structure of excited state absorption spectra.^{123,124} In their case, an excited state aromatic compound has an absorption spectrum similar to a ground state aromatic analogue, and vice versa for excited state antiaromaticity. A further introduction to excited state aromaticity is given in ??.

Table 1.1: Effect of topology, π -electron count and electronic state on (anti)aromatic character.

		Ground state		Excited state	
		$4n$	$4n + 2$	$4n$	$4n + 2$
<i>Hückel</i>	Antiaromatic	Aromatic	Aromatic	Antiaromatic	
<i>Möbius</i>	Aromatic	Antiaromatic	Antiaromatic	Aromatic	

1.4 The limits of electron delocalisation

Aromaticity can be considered the limit of electron delocalisation in molecules: the ring-current model leads us to imagine that the π -electrons are freely circulating around the entire conjugation path. However, cyclic conjugation is not the sole requirement for aromaticity: the cycloparaphenylenes (CPP) and cycloparaphenyleneacetylenes (CPPA) do not exhibit

1.4. The limits of electron delocalisation

measurable macrocyclic aromaticity around their peripheries,* as evidenced by their benzenoid NMR spectra.^{126–128} Indeed, it is only upon oxidation to the dication that a ring current is observed in [8]-CPP.¹²⁹ Similarly to homoaromaticity in charged molecules, it seems that oxidation disrupts the ground state electronic character (8 isolated benzene rings) and permits enhanced delocalisation (a [32]-annulene dication with 30 π -electrons).

We are led to the inevitable question: if CPP does not exhibit macrocyclic aromaticity, how can porphine be aromatic? Porphine has three sources of aromatic stabilisation, all calculated to be of roughly equal weight ($\sim 80 \text{ kJ mol}^{-1}$ BLW-ASE (block-localised wavefunction)): the [18]-annulene pathway and two pyrroles.⁴⁶ The pyrrole aromaticity is not entirely ‘switched off’ in favour of the [18]-annulene circuit, since there are still local pyrrolic ring currents. The same calculations predict a BLW-ASE for benzene of about 120 kJ mol^{-1} , and for isolated pyrrole of about 70 kJ mol^{-1} .⁴⁶

There are two key differences between the CPP(A)s and porphine: first, there is much more ASE to be lost (about 50 kJ mol^{-1}) by (partial) disruption of the local aromaticity of benzene than of pyrrole. Second, in the absence of an [18] π -electron circulation in porphine, the 12 non-pyrrolic π -electrons of the circuit are localised: essentially, there is a Pauling resonance argument for delocalising these additional electrons through macrocyclic aromaticity. In contrast, CPP has no localised electrons, and $[n]$ -CPPA has a $6n:4n$ ratio of aromatic:static electrons. If a macrocyclic ring current were to be established in $[n]$ -CPPA, only 4 π -electrons from each benzene would be involved, immediately negating the electron-counting benefit of including $2n$ acetylene electrons in the macrocyclic aromatic circuit.¹³⁰

As will be discussed in the introductions to Chapters ??, ?? and ??, large aromatic molecules are of interest because they may exhibit novel quantum effects, such as a Aharonov-Bohm oscillations of the ring current direction as a function of magnetic field.^{130,131} Such oscillations, introduced in more detail in ??, could result in magnetic field control of conductance through a molecular junction.^{132,133} Intriguingly, at high magnetic fields it has been calculated that molecular ring currents will reverse direction,^{134,135} just like the experimental observations in metal rings.¹³⁶

*Taubert et al. have calculated the magnitude of macrocyclic ring currents in [6]-CPP to [11]-CPP and report paratropic and diatropic currents for [6]-CPP and [7]-CPP, respectively. These ring-currents do not significantly affect NICS(0) at the CPP ring centres (-2.1 ppm and -1.9 ppm for [6]- and [7]-CPP, respectively). The reversal of the calculated current direction between [6]- and [7]-CPP is surprising because both CPPs are, formally, $[4n]$ all-*cis* annulenes. In contrast, the dianions ($[4n+2]$ π -electrons) of all the CPPs studied are aromatic according to NICS(0).¹²⁵

1. Introduction

Aromaticity and antiaromaticity are predominantly features of molecules with even numbers of electrons. For those with odd-numbers of electrons, such as radical cations and anions, the focus for studies of electron delocalisation is the radical electron/hole, or polaron. As we shall introduce more thoroughly in ??, the extent of charge (or spin) delocalisation is an important predictor of molecular properties in a device: with long delocalisation lengths, coherent transport becomes possible, preserving the quantum state of an injected electron or hole.¹³⁷ In contrast, shorter delocalisation lengths can still transmit charge over long distances along a molecular wire, through a stepwise hopping process.¹³⁷ Charge delocalisation has been reported to be ‘extreme’ (across up to seven porphyrin units, 7.5 nm) in monoalkyne-linked linear porphyrin oligomer radical cations and anions.^{138,139} Polyfluorenes (**PF**) have been extensively studied, and seem to have a radical anion delocalisation length of 3–5 fluorene units.^{140–142} For poly(3-decylthiophene) (**P3DT**), the polaron delocalisation length is remarkably long: 11.5 units for an anion, or 8.7 units for a cation,¹⁴³ though in terms of spatial extent (4–5 nm) these distances are similar to those for **PF**. In contrast, the polaron delocalisation length is limited to 2–3 monomer units in a poly(phenylenevinylene) (**PPV**) radical anion.^{142,144}

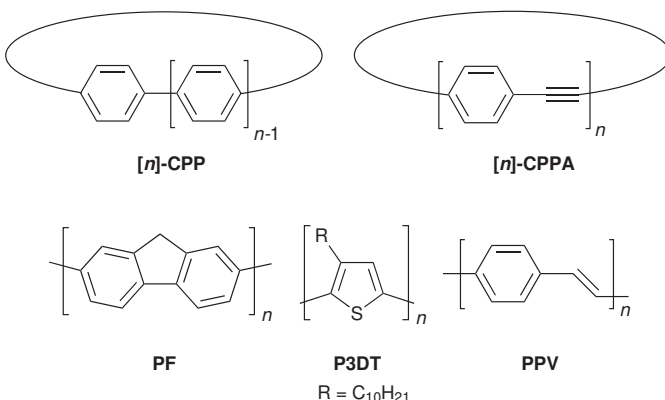


Figure 1.18: Examples of conjugated polymers.

Charge delocalisation is controlled by two competing effects: the conjugated π -system efficiently delocalises charge, but its efforts are frustrated by the presence of conjugation breaking defects. These defects can be kinks and twists in the oligomer chain,¹⁴⁵ or can arise from a more dynamic vibrational relaxation following polaron formation: electron-phonon coupling. In this second case, a short segment of the oligomer chain becomes more strongly conjugated (lower BLA) and thus encourages charge localisation within this region.¹⁴³ Overall, polaron delocalisation depends on π -conjugation, oligomer flexibility, and the absence of charge-localising vibrations.

1.5 Prospective

The remainder of this thesis starts by considering perhaps the simplest case of delocalisation in butadiyne-linked porphyrin oligomers: the resonance energy of the neutral dimer **I-P2** (Chapter 2). The resonance energy is determined from the experimentally determined height of the torsion barrier for rotation of porphyrins around the butadiyne link. Chapter 2 also serves to introduce some of the photochemistry of porphyrins.

Next, we explore the chemistry of the even π -cations of the [6]-porphyrin nanoring **c-P6** and its template complex **c-P6•T6** (??). Although the nanoring does not exhibit global aromaticity (i.e. around the nanoring circumference) in its neutral oxidation state, after oxidation it is shown to obey Hückel's law. **c-P6** exhibits aromaticity and antiaromaticity in its 6+ and 4+ oxidation states, respectively. It is even possible to generate the 12+ cation of the nanoring: this oxidation state corresponds to six antiaromatic ([16]- π) porphyrin subunits, and global (anti)aromaticity is not prominent. These conclusions are developed from DFT and experiment.

We next turn to an exploration of charge and spin delocalisation in the radical cations of a series of linear (**I-P1** to **I-P6**), cyclic (**c-P6** and **c-P6•T6**) and tubular (**t-P12•T6₂**) porphyrin oligomers (??). By using spectroelectrochemistry, DFT, and EPR, we show that the cation is delocalised over just two or three porphyrin units.

The thesis concludes with two short chapters which each extend the study of aromaticity in porphyrin nanorings. In ?? we ask whether porphyrin nanorings exhibit ES(A)A. Although DFT suggests that nanorings smaller than **c-P8** do have ES(A)A, initial photophysical experiments do not reveal any physical manifestations. In the final chapter (??) we use DFT to calculate the effect of removing a single acetylene (C_2) unit from **c-P6** – does the nanoring still obey Hückel's rules when two π -electrons are removed, with an accompanying reduction in symmetry? The resulting molecule, with asymmetric conjugation paths, is interesting for studies on quantum interference. This chapter is entirely computational: synthetic efforts towards the truncated nanoring are under way independently.

I do not know what I may appear to the world, but to myself I seem to have been only like a boy playing on the sea-shore, and diverting myself in now and then finding a smoother pebble or a prettier shell than ordinary, whilst the great ocean of truth lay all undiscovered before me.

— Isaac Newton, as quoted in Memoirs of the Life, Writings, and Discoveries of Sir Isaac Newton (1855) by David Brewster (Volume II. Ch. 27)

2

Experimental and computational evaluation of the barrier to torsional rotation in a butadiyne-linked porphyrin dimer

Parts of this chapter were published in: M. D. Peeks, P. Neuhaus and H. L. Anderson,

'Experimental and Computational Evaluation of the Barrier to Torsional Rotation in a

Butadiyne-Linked Porphyrin Dimer', *Phys. Chem. Chem. Phys.*, 2016, **18**, 5264–5274.

2.1 Abstract

The barrier to torsional rotation in a butadiyne-linked porphyrin dimer in solution has been determined by variable temperature UV-Vis-NIR spectroscopy: $\Delta H = (5.27 \pm 0.03) \text{ kJ mol}^{-1}$, $\Delta S = (10.69 \pm 0.14) \text{ JK}^{-1} \text{ mol}^{-1}$. The value of ΔH agrees well with theoretical predictions. Quantum chemical calculations (DFT) were used to predict the torsion angle dependence of the absorption spectrum, and to calculate the vibronic fine structure of the $S_0 \rightarrow S_1$ absorption for the planar dimer, showing that the absorption band of the planar conformer has a vibronic component overlapping with the $\langle 0|0 \rangle$ absorption of the perpendicular conformer. The torsion barrier in the porphyrin dimer is higher than that of 1,4-diphenylbutadiyne (calculated $\Delta H = 1.1 \text{ kJ mol}^{-1}$). Crystallographic bond lengths and IR vibrational frequencies confirm that there is a greater contribution of the cumulenic resonance form in butadiyne-linked porphyrin dimers than in 1,4-diphenylbutadiyne. The DFT frontier orbitals of the twisted conformer of the porphyrin dimer are helical, when calculated in the absence of symmetry. The helical character of these orbitals disappears when D_{2d} symmetry is enforced in the 90° twisted conformer. Helical representations of the frontier orbitals can be generated by linear combinations of the more localised orbitals from a symmetry-constrained calculation but they do not indicate π -conjugation. This work provides insights into the relationship between electronic structure and conformation in alkyne-linked conjugated oligomers.

2.2 Introduction

Molecules with extended π -conjugation are of wide interest, both as ingredients in molecular electronic and optical materials,^{146,147} and as molecular wires for creating nanoscale electronic devices.^{148–151} Conjugated oligomers and polymers have been constructed by linking aromatic monomer units with a wide variety of π -conjugated bridges.¹⁵² The properties of these oligomers are critically dependent on the molecular conformation because any twist in the π -system can dramatically reduce the coherent electronic coupling through the bridge. Conformational heterogeneity can thus attenuate the ability of a conjugated molecule to transport charge or electronic excitation. Several workers have explored the relationship between conformation and function in different types of molecular wire.^{15,152–159} Conjugated butadiyne-linked porphyrin oligomers have been actively investigated for more than twenty

2. Experimental and computational evaluation of the barrier to torsional rotation in a butadiyne-linked porphyrin dimer

years,^{18,19,21,160,161} but the barrier to torsional rotation around the butadiyne link has yet to be determined experimentally. In this chapter, we present a time-dependent density functional theory (TD-DFT) evaluation of the electronic excitations of the porphyrin dimer as a function of inter-porphyrin torsion angle, and use variable temperature (VT) UV-Vis-NIR spectroscopy to determine the torsion barrier. Our experimental results permit the accurate simulation of conformational dynamics in this, and similar, systems. Our (TD-)DFT results provide insights into the nature of bonding and electronic excitations in butadiyne-linked oligomers.

Porphyrin-based molecular wires have been widely investigated for their potential applications in functional materials,² as dyes for two-photon absorption,^{162,163} as models for biological photosystems (e.g. light-harvesting photosystem 2)¹⁶⁴ and as wires for single-molecule charge transport.^{165–167} The Anderson group, and others, have prepared a wide variety of *meso–meso* butadiyne-linked porphyrin architectures, including linear oligomers,^{21,22,161,168} nanorings^{25,169} and supramolecular complexes.^{21,23,170} Other linking groups have also been explored: *meso–meso* alkynylene,¹⁶⁰ vinylene,¹⁷¹ phenylenes,^{172–174} and direct porphyrin connection via oxidative coupling at the β and *meso* positions,¹⁷⁵ among many others.

The *meso–meso* butadiyne link permits strong inter-porphyrin electronic coupling and the extension of conjugation upon oligomer homologation is most apparent in the progressive bathochromic shift of the lowest energy optical transition ($S_0 \rightarrow S_1$, 625–850 nm, Q-band, Figure 2.1). However, the butadiyne link also permits torsional heterogeneity, with a continuous range of torsion angles (θ) between the porphyrin chromophores. The length of the butadiyne bridge is sufficient to avoid any steric repulsion between the opposing β hydrogens of the porphyrins (denoted "X" in Table 2.1), thus the lowest energy conformer is planar ($\theta = 0^\circ$). The energy difference between the perpendicular and planar conformers reflects the bridge-mediated resonance stabilisation energy between the porphyrins. The torsional heterogeneity contributes towards the increasing width of the Q-band absorption with increasing oligomer length (Figure 2.1).

Previous semi-empirical and DFT calculations have predicted that the lowest energy conformation of **P2** is planar ($\theta = 0^\circ$). These calculations gave a torsional energy barrier (ΔE) of about 3–4 kJ mol^{−1} (Table 2.2, Figure 2.2) between $\theta = 0$ and 90° ,^{30,161,176} which is in the range of $k_B T$ at room temperature (2.48 kJ mol^{−1}), thus it is anticipated

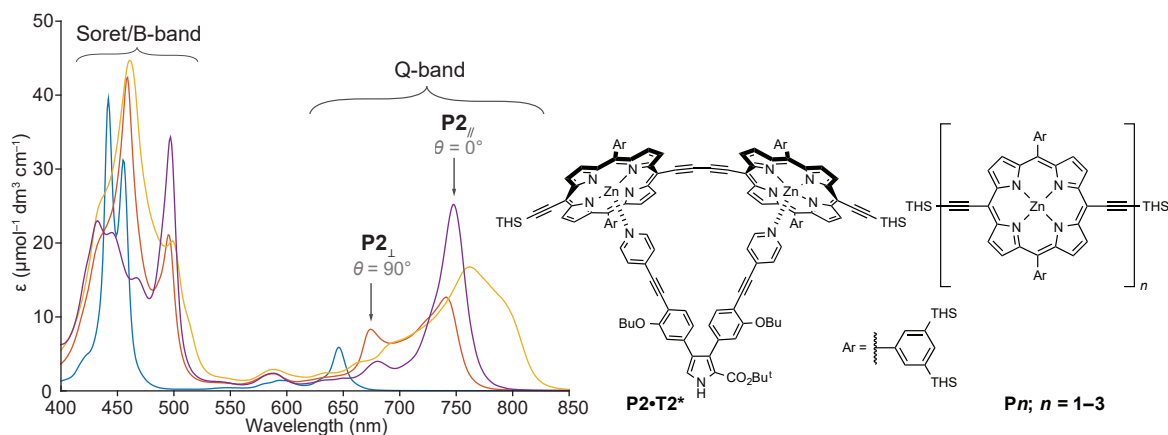


Figure 2.1: Absorption spectra of linear oligomers: monomer **P1** (blue), dimer **P2** (red), trimer **P3** (yellow) and planar dimer complex **P2 • T2⁺** (purple). (Solvent: $\text{CH}_2\text{Cl}_2:\text{THF}:\text{pyridine}$ 10:10:1, except **P2 • T2⁺**: CH_2Cl_2 . THS = trihexylsilyl.)

that all torsion angles are populated at room temperature. The barrier height was not significantly affected by the use of a range-separated DFT functional (CAM-B3LYP),¹⁷⁷ an effective core potential, or a solvent model (Table 2.2). The torsion profile for the butadiyne linked dimer **P2** contrasts with that for the corresponding monoalkyne linked dimer:¹⁶⁰ in that case, coplanarity is disfavoured by the steric clash between porphyrin β protons, and the DFT equilibrium torsion angle is about 34° (Figure 2.2). The ΔE between the equilibrium geometry and the perpendicular 90° conformer is around 5 kJ mol^{-1} , greater than that in butadiyne linked **P2**, and indicating increased conjugation across the linker. These computational results on **C₂-P2** are in agreement with those found in several other studies, reviewed and contributed to by Rintoul et al.,¹⁷⁸ who note that the computational equilibrium torsion angle ($\sim 35^\circ$) is much greater than that expected from the narrow, redshifted absorption spectrum and than the angles observed in crystal structures ($0-20^\circ$).

Computational work³⁰ (TD-DFT calculations, reproduced in this work, Figure 2.5) has shown that the visible electronic transitions of the butadiyne-linked porphyrin dimer exhibit a strong dependence on interporphyrin torsion angle θ ; as θ increases from 0 to 90° the Q-band transition is hypsochromically shifted. Torsion angle-dependence is also apparent in the B-band, albeit in the presence of several overlapping transitions.

The torsion-dependence of the Q-band absorption wavelength has been exploited to selectively excite populations of molecules with different conformations. The wavelength of fluorescence emission is also dependent on the torsion angle. Analysis of fluorescence emission and excitation spectra shows that the S_1 state has a much higher torsion barrier

2. Experimental and computational evaluation of the barrier to torsional rotation in a butadiyne-linked porphyrin dimer

Table 2.1: Molecular structures referred to in Table 2.2 and in the present study

#	M	R	X	Y
19a	Ni	H	Et	H
19b	Zn	H	H	H
19c	Zn	Ph	H	C ₂ H
19d	Zn	Ph	H	C ₂ SiMe ₃
19e	Zn	H	H	C ₂ H
P2	Zn	Ar [†]	H	C ₂ THS [‡]

† Ar = 3,5-bis(trihexylsilyl) as defined in Figure 2.1.

‡ THS = trihexylsilyl.

Table 2.2: Calculated barriers, ΔE , to torsional rotation in butadiyne-linked porphyrin dimers

Molecule	Method	ΔE (kJ mol ⁻¹)	Ref
19a	VWN and BP86	~63	[176]
19b	AM1	~4	[161]
19c	B3LYP/6-31G*	2.8	[30]
19d	B3LYP/6-31G*/LANL2DZ	3.1 [†]	This work
19d	TPSSh/6-31G*/LANL2DZ	3.7 [†]	This work
19d	CAM-B3LYP/6-31G*	1.3 [†]	This work
19d	CAM-B3LYP/6-31G* [‡]	2.3 [†]	This work
19d	B3LYP/def2-SV(P)	2.8 [†]	This work
19e	B3LYP/6-31G*	2.6 [†]	This work

† No zero-point energy (ZPE) correction applied.

‡ PCM THF solvent model.

(16 kJ mol⁻¹) than the electronic ground state (S_0).³⁰ Perpendicular conformers which are excited to S_1 tend to planarise prior to emission, unless solvent viscosity retards the rotation.^{30,179–181} The torsion angle has also been found to influence the two-photon absorption (2PA) cross-section and the singlet oxygen ($^1\text{O}_2$) yield. Planar conformers have stronger two-photon absorption,¹⁶³ larger third-order optical non-linearities¹⁸² and higher charge-mobilities,^{183,184} and they are more efficient oxygen sensitizers because intersystem crossing ($S_1 \rightarrow T_1$) is faster than in twisted conformers.¹⁷⁹

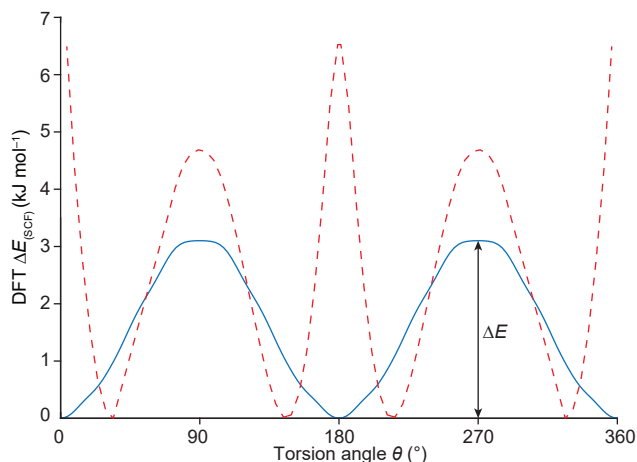


Figure 2.2: Calculated (B3LYP/6-31G*/LANL2DZ) energy profile for butadiyne torsion in **P2**, model **19d** (blue). The red dashed line shows the torsion profile (B3LYP/6-31G*) for a monoalkyne linked analogue of **P2** (substitution pattern corresponding to model **19b**). θ is the angle between the mean planes of each porphyrin, defined by the 24 non-hydrogen atoms in each macrocycle. The indicated ΔE is the torsional barrier for **P2** which is under discussion in this chapter.

The torsion angle can be constrained to enforce coplanarity by the preparation of supramolecular complexes, such as ladder complexes with a bidentate ligand (e.g. DABCO or 4,4'-bipyridine),²³ or simple 1:1 complexes between oligomers and designed templates, such as **T2** (Figure 2.1).^{30,184} Fixing the torsion angle results in the expected bathochromic shift and sharpening of the Q-band (Figure 2.1), as the conformation is restricted to a librational range of angles around $\theta \approx 0^\circ$.

Interestingly, Aida et al. prepared tetrameric cages from *meso*-pyridyl substituted butadiyne-linked porphyrin dimers.¹⁸⁵ They found that the cage composed of dimer units with perpendicular porphyrins was favoured, due to the resulting cancellation of the pyridine dipole moments. This result showed that the torsion barrier in the butadiyne-linked dimer is low enough to be overcome by a dipole-based conformational preference.¹⁸⁵

The aim of this chapter is to experimentally determine the barrier to torsion in porphyrin dimer **P2** using VT UV-Vis-NIR spectroscopy and to understand how torsional rotation alters the electronic structure of this molecule. After presenting the VT UV-Vis-NIR results, we will discuss our theoretical analysis of the electronic excitations. With the help of this theoretical analysis, we will extract thermodynamic parameters using a van't Hoff analysis. We will use evidence from IR spectroscopy and bond-length alternation to discuss the resonance stabilisation of the planar conformer. Finally, we discuss our observation of helical frontier orbitals and natural transition orbitals in DFT calculations.

2. Experimental and computational evaluation of the barrier to torsional rotation in a butadiyne-linked porphyrin dimer

2.3 Methods

2.3.1 Synthesis and spectroscopy

Porphyrin compounds were prepared as described previously.^{183,186} Oligomers **PN** with trihexylsilyl (THS) solubilising groups on the *meso*-aryls were used throughout this study, since THS porphyrins exhibit excellent solubility and a low propensity towards aggregation. Room temperature UV-Vis-NIR spectra were recorded using a Perkin-Elmer Lambda 20 with a 1 cm quartz cuvette. Variable temperature UV-Vis-NIR spectra were recorded using a Perkin-Elmer Lambda 1050 and an Oxford Instruments LN₂ optical cryostat, with 1 cm and 1 mm Infrasil Quartz cuvettes (Starna). In all cases, freshly mixed CH₂Cl₂:THF:pyridine (10:10:1) was used as the solvent mixture. CH₂Cl₂ and THF were dried over activated alumina before use. CH₂Cl₂ contained amylene (50–150 ppm) as a stabiliser; THF was unstabilised. Variable temperature UV-Vis-NIR experiments were performed across a wide concentration range (0.8 µM, 1.6 µM and 58.5 µM) to confirm the absence of thermally-induced aggregation. Absorbances were not corrected for concentration change due to thermal contraction of the solvent, since the ratio of absorbances is not affected by concentration. Emission spectra were collected using an ISA Fluoromax-2 Fluorimeter. Infrared spectra were collected using a Bruker Tensor 27 FT-IR spectrometer in ATR mode with neat sample, with 2 cm⁻¹ resolution at 293 K.

2.3.2 Computational methods

All (TD-)DFT calculations were conducted using Gaussian09/D.01.¹⁸⁷ The B3LYP density functional¹⁸⁸ was used in conjunction with the 6-31G* basis set,^{189–192} with the LANL2DZ ECP^{193,194} on Zn as indicated. For computational tractability, truncated model compounds were used. The potential-energy surface scan and TD-DFT calculations used a model of **P2** with phenyl substituents in place of the *meso*-aryls, and trimethylsilyl protecting groups as the acetylene end-groups, and C₁ symmetry, **19d**. Further truncated models were used for the calculation of the vibronic fine structure of the Q-band transitions and vibrational frequencies: the *meso*-aryls and the trimethylsilyl acetylene protecting groups were replaced by hydrogens, **19e**. These calculations were then conducted in D_{2h} and D_{2d} symmetry for planar and perpendicular conformers respectively.

2.4. Results and discussion

The potential energy surface was calculated by varying the interporphyrin torsion angle in 2.5° increments and, while holding the torsion coordinate fixed, relaxing the remainder of the structure. The resulting ΔE_{SCF} is used for comparison: the zero-point vibrational contribution to the energy has been neglected unless indicated otherwise. Vibrational frequencies (calculated analytically, with the harmonic oscillator model) were scaled by a multiplicative factor of 0.96.

Unless otherwise specified, orbital isosurfaces are depicted using the default threshold settings in the Chimera¹⁹⁵ program. Namely, the thresholds are placed symmetrically about zero, at a value which encompasses 99% of the voxels on either side of zero.

2.4 Results and discussion

2.4.1 Experimental VT UV-Vis-NIR spectroscopy

Since the calculated torsion barrier ΔE is of the order of $k_B T$ at room temperature, we envisioned that VT UV-Vis-NIR spectroscopy would probe the equilibrium between twisted and planar conformers. Indeed, dramatic changes in the UV-Vis-NIR spectrum of **P2** ($\sim 59 \mu\text{M}$, $\text{CH}_2\text{Cl}_2:\text{THF}:\text{pyridine}$ 10:10:1) were observed upon cooling within the solvent liquid range (298–173 K, Figure 2.3). Below 180 K, discontinuous changes in the spectra are observed, which we attribute to changes in bulk solvent properties at temperatures close to the glass transition temperature.¹⁹⁶

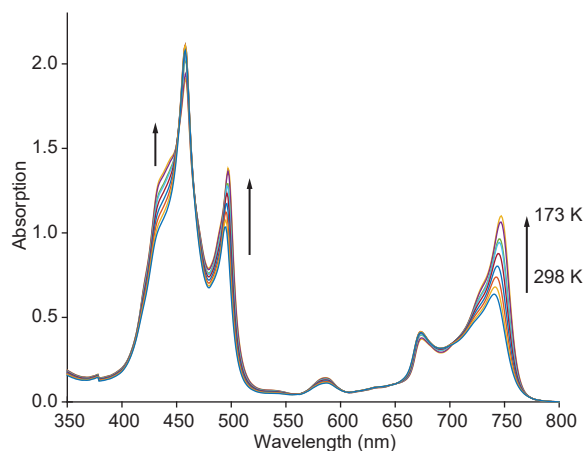


Figure 2.3: Variable temperature (298–173 K) absorption spectra of porphyrin dimer **P2** in $\text{CH}_2\text{Cl}_2:\text{THF}:\text{pyridine}$ (10:10:1), concentration ca. $59 \mu\text{M}$, path length 1 mm.

Previous work has shown that temperature-dependent changes in the absorption spectra of butadiyne-linked porphyrin oligomers can be caused by aggregation,^{197,198} but as noted in

2. Experimental and computational evaluation of the barrier to torsional rotation in a butadiyne-linked porphyrin dimer

the Methods, we were able to exclude the presence of aggregation by selection of appropriate solvent and solubilising side-chains. VT experiments performed on the porphyrin monomer **P1** in the same solvent mixture showed that, within the temperature range 298–163 K, there is no thermochromic shift of the Q-band absorption λ_{\max} (Figure 2.4).

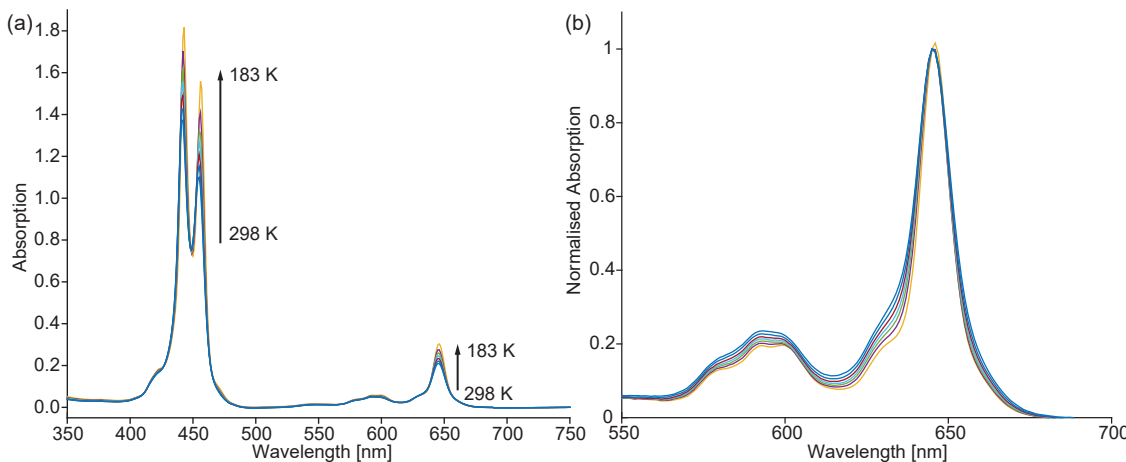


Figure 2.4: VT UV-Vis spectra of monomer **P1** in $\text{CH}_2\text{Cl}_2:\text{THF}:\text{pyridine}$ 10:10:1, (a) full spectrum in temperature range 298–77 K (b) expansion of Q-band region in temperature range 298–163 K.

When a solution of **P2** is cooled, its UV-Vis-NIR spectrum exhibits several changes (Figure 2.3): the red edge of the Q-band becomes more intense (~740 nm; planar conformations, $\theta \approx 0^\circ$), at the expense of a slight decrease in intensity on the blue edge (675 nm; perpendicular conformations, $\theta \approx 90^\circ$). We can be confident in our assignment of the absorbance at 675 nm to perpendicular conformers thanks to measurements of the emission of twisted dimer conformers in viscous solution by Kuimova et al.,¹⁸⁰ who found that highly viscous solvents inhibited excited state planarisation. The resulting emission, predominantly from twisted conformers, occurred bathochromically to the “shoulder” on the high-energy side of the Q-band absorption.

The absorption at 570 nm, assigned with the help of TD-DFT to near-planar conformers (see later), increases intensity on cooling. In the Soret/B-band, a sharpening and intensification of the absorption on the red edge is observed (~490 nm). This band can thus also be assigned to near-planar conformers. Before discussing the van't Hoff analysis of the VT UV-Vis-NIR of **P2**, we will further develop our understanding of the absorption spectra using TD-DFT.

2.4.2 Calculated electronic transitions as a function of torsion angle

We computed the electronic excitations for different torsion angles using TD-DFT (B3LYP/6-31G*/LANL2DZ) (Figure 2.5). The results agree with earlier published work.³⁰ The transition dipole moments for the lowest energy part of the Q-band are polarised along the butadiyne (long, x) axis, as observed experimentally.^{199,200} Analysis of the angle dependence of the Q-band excitation energy reveals a relationship to $\cos \theta$: i.e., the projection of the porphyrin planes (Figure 2.6), as given by equation (2.1):

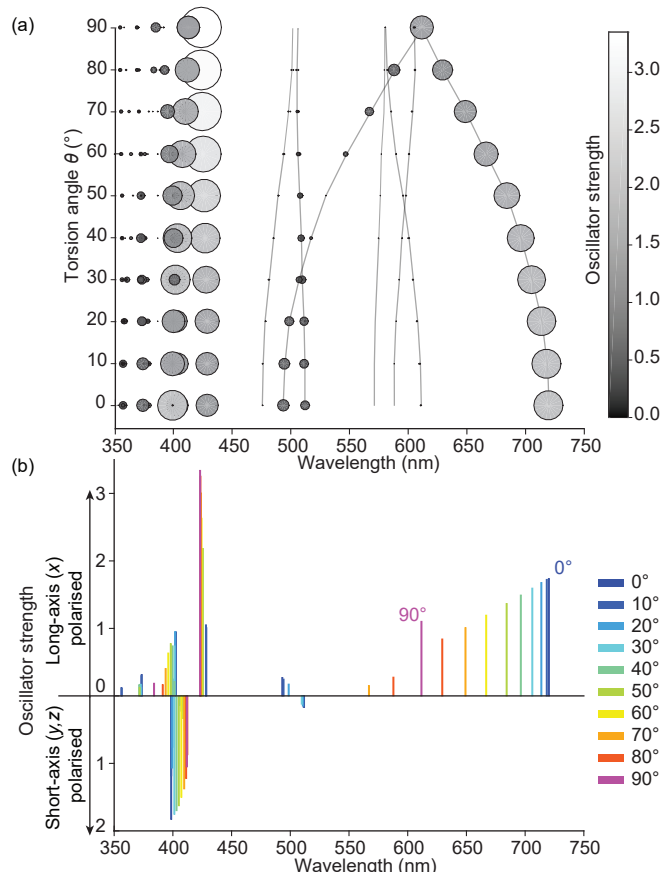


Figure 2.5: Calculated (TD-B3LYP/6-31G*/LANL2DZ) vertical excitation energies in the UV-Vis-NIR region for different torsion angles in a model P2 (19d). (a) Calculated wavelength vs. torsion angle. Faint grey lines (only shown for the Q-bands) connect corresponding states, comprising a Walsh diagram; circle size is proportional to oscillator strength, as is the circle shading. (b) Calculated wavelength vs. oscillator strength. Transitions with oscillator strength <0.1 are not included. Bars above the x-axis correspond to transitions polarised along the long molecular axis (x, butadiyne axis) of the molecules. Bars below the x-axis correspond to transitions polarised along either the y or z (short) molecular axes.

$$E_Q \approx E_{\perp} - (E_{\perp} - E_{\parallel}) \cdot \cos \theta \quad (2.1)$$

2. Experimental and computational evaluation of the barrier to torsional rotation in a butadiyne-linked porphyrin dimer

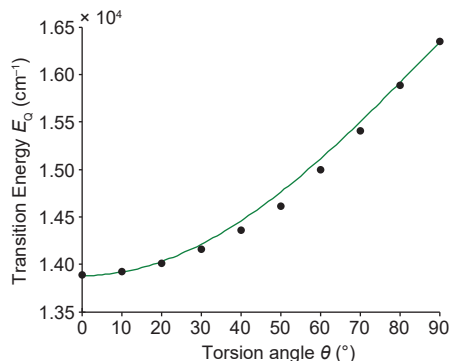


Figure 2.6: Comparison of TD-DFT calculated $S_0 \rightarrow S_1$ vertical excitation energy (blue) vs. a predictive model based on the projection of the porphyrin planes (green) (Eqn. (2.1)).

where E_Q is the Q-band absorption energy for a conformer with inter-porphyrin torsion angle θ . E_{\parallel} and E_{\perp} are the limiting energies for planar (low energy) and perpendicular (high energy) conformers, respectively. This function readily relates absorption energy to the overlap of the porphyrin π -systems along the butadiyne and shows that E_Q is most sensitive to θ when $\theta \approx 90^\circ$.

The calculated oscillator strength of the lowest energy transition is surprisingly high for the 90° conformer (Figure 2.5b), contrasting its gradual decrease with increasing θ between 0 – 80° . This result does not appear to be a simple computational artefact: the increase of oscillator strength is gradual from 85 – 90° (Figure 2.7). Close examination of the TD-DFT results reveals that, on twisting from 0 – 90° , the second-lowest energy x-axis (long axis) polarised transition is progressively redshifted until it becomes degenerate with the lowest energy transition (Figure 2.5a). This analysis further reveals that the weak absorption centred at ~ 580 nm in the experimental spectrum (Figure 2.1) arises predominantly from planar conformers, and contains components polarised along both the long (x) and short (y) molecular axes. A detailed discussion of TD-DFT results and orbital/state correlations as a function of torsion angle has been published previously by Winters et al., and our computational results are in complete agreement with theirs.³⁰

The high oscillator strength of the Q band of the perpendicular conformer ($\theta = 90^\circ$) provides a partial explanation for the peak observed in the absorption spectrum at 675 nm (Figures 2.1 and 2.3). However, a further contribution appears likely because the peak at 675 nm persists at low temperature, with similar relative intensity to the planar conformer as at room temperature. Even at 78 K, at which temperature occupation of the perpendicular state should be thermally inhibited, there is a discrete absorption at ~ 675 nm (Figure 2.8).

2.4. Results and discussion

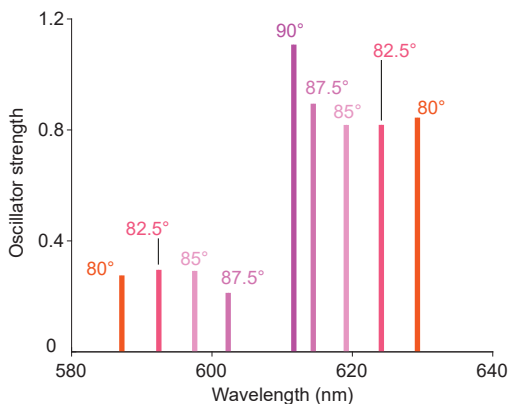


Figure 2.7: TD-DFT (B3LYP/6-31G*/LANL2DZ) calculated excitation energies and oscillator strengths for **P2** (model **19d**) as a function of inter-porphyrin torsion angle

Room temperature emission spectra of **P2** and **P2•T2** (Figures 2.9a and 2.9b) show a similar shoulder on the red edge of the main emission band. Therefore we assign this shoulder to a vibronic contribution of the planar conformer, with the support of computational results described in the next section.

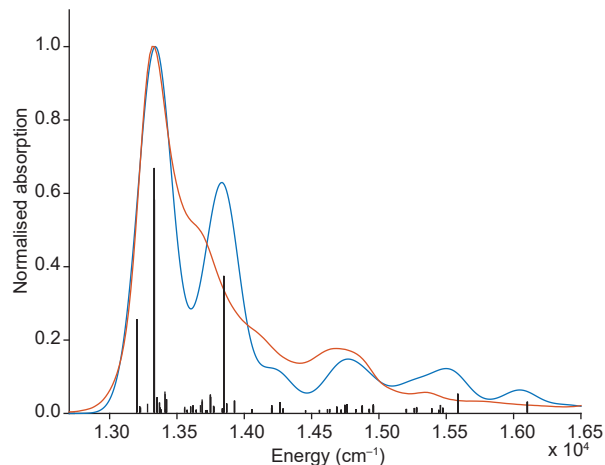


Figure 2.8: (red) Absorption spectrum of Q-band region (600–800 nm) of **P2** in frozen solution ($\text{CH}_2\text{Cl}_2:\text{THF}:\text{pyridine}$ 10:10:1) at 78 K; (blue) calculated (B3LYP/6-31G* Franck-Condon/Herzberg-Teller approximation) vibronic structure of Q-band absorption for planar **P2**, model **19e**; (sticks) vibronic transitions; transitions with low relative intensity are not plotted. The $\langle 0|0 \rangle$ transition in the computational result was shifted in energy to match the low-energy peak in the experimental spectrum (red).

2. Experimental and computational evaluation of the barrier to torsional rotation in a butadiyne-linked porphyrin dimer

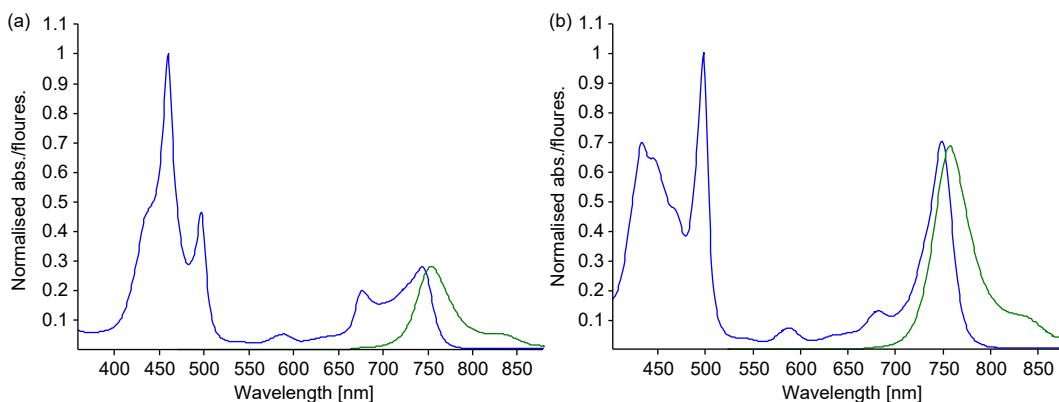


Figure 2.9: Absorption (blue) and fluorescence (green) of (a) **P2** ($\text{CHCl}_3 + 1\%$ pyridine), $\lambda_{\text{ex}} = 450$ nm and (b) **P2•T2** (CHCl_3), $\lambda_{\text{ex}} = 450$ nm, $\lambda_{\text{max}}(\log_{10} \epsilon)$: 749 (5.297), 682 (4.574), 588 (4.324), 498 (5.452), 434 (5.295).

2.4.3 Vibronic contribution to the Q-band electronic transition

We used the Franck-Condon (FC) and Herzberg-Teller (HT) approximations as implemented in Gaussian09/D.01 to calculate the vibronic absorption spectrum for the $S_0 \rightarrow S_1$ transition in planar **P2**.^{201,202} The calculation was restricted to excitations originating from the vibrational ground state of S_0 , thus treating the vibronic spectrum as temperature independent. This calculation gave a predicted spectrum which is in remarkably close agreement to the experimental spectrum of **P2** recorded at 78 K (Figure 2.8). At this temperature the near-planar conformers of **P2** are expected to be dominantly populated. The major vibronic bands arise from intra-porphyrin collective stretching modes, and do not appear to involve nuclear displacements on the butadiyne link (see Figure 2.10). The vibronic band which we calculate at $\sim 390 \text{ cm}^{-1}$ from the $\langle 0|0 \rangle$ transition has also been experimentally characterised by Camargo et al. in **P1**, at 380 cm^{-1} .²⁰³ We used the computational vibronic spectrum to firmly assign the absorption at 675 nm in (planar) **P2•T2** (Figure 2.1) to a vibronic contribution. Similarly, the anomalously increased intensity at the blue edge of the Q-band (~ 675 nm) in the experimental spectra of **P2** at room temperature (Figure 2.1) is partially attributed to this vibronic contribution, in addition to the relatively high oscillator strength of the overlapping perpendicular absorption. The significant overlap between the absorption of the twisted conformer and that of a vibronic band of the planar conformer rationalises previous results where wavelength-selective excitation of the twisted conformer appeared to result, additionally, in excitation of the planar conformer.^{30,163}

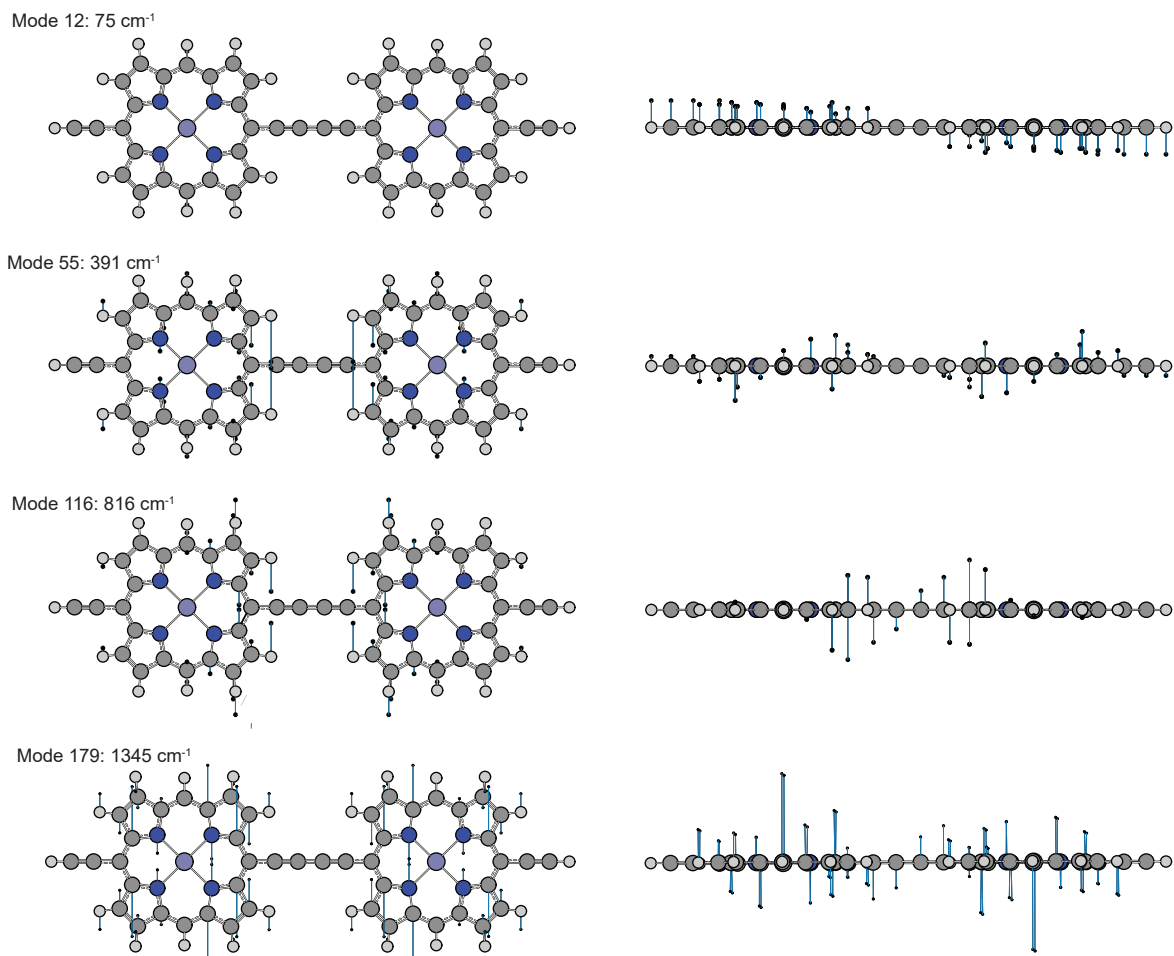


Figure 2.10: Normal modes of S_1 state of **P2** (model 19e) associated with major vibronic bands.

2.4.4 van't Hoff analysis of experimental VT UV-Vis-NIR data

The experimental VT UV-Vis-NIR data were subject to a van't Hoff analysis of the equilibrium constant for a simple two-state model comprising near-planar and near-perpendicular conformers, **P2**_{||} ($\theta \approx 0^\circ$) and **P2**_⊥ ($\theta \approx 90^\circ$) with concentrations proportional to the absorbances at 750 and 675 nm, respectively, weighted by the TD-DFT oscillator strengths for the 0° and 90° transitions.[‡] The vibronic contribution of the planar conformer to the absorption at 675 nm (mostly perpendicular conformer) was subtracted. The relative magnitude of this vibronic contribution was assumed to be temperature-invariant and was calculated from the ratio of peak heights in the spectrum of **P2** at 78 K.

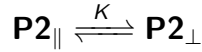
[‡]We also used the van't Hoff equation without weighting the absorbances at 750 and 675 nm to the calculated oscillator strengths. This approach does not change the resulting value of ΔH ($(5.27 \pm 0.03)\text{ kJ mol}^{-1}$), but it gives a higher value of ΔS ($(14.42 \pm 0.14)\text{ JK}^{-1}\text{ mol}^{-1}$); thus, $\Delta G_{298\text{ K}}$ becomes $(0.98 \pm 0.05)\text{ kJ mol}^{-1}$

2. Experimental and computational evaluation of the barrier to torsional rotation in a butadiyne-linked porphyrin dimer

The equilibrium constant at each temperature was thus calculated according to equation (2.2):

$$K = \frac{f_{\parallel}}{f_{\perp}} \cdot \frac{A_{\perp}}{A_{\parallel}} = \frac{f_{\parallel}}{f_{\perp}} \cdot \frac{A_{675} - A_{750} \cdot x_{vibr}}{A_{750}} \quad (2.2)$$

where K is the equilibrium constant for:



A_{\parallel} and A_{\perp} are the absorbances for planar and perpendicular conformers, respectively. f_{\parallel} and f_{\perp} are the TD-DFT oscillator strengths for planar and perpendicular conformers, respectively ($\frac{f_{\parallel}}{f_{\perp}} = 1.574$). x_{vibr} is the ratio of the intensities of the planar $\langle 0|0 \rangle$ absorption and its vibronic contribution (at $\sim 1350 \text{ cm}^{-1}$ separation) in the experimental 78 K spectrum of **P2** ($x_{vibr} = 0.186$). The ratio of TD-DFT oscillator strengths (1.574) is consistent with the ratio of estimated experimental extinction coefficients for the planar and perpendicular conformers ($\frac{\epsilon_{\parallel}}{\epsilon_{\perp}}$) was estimated by comparing the absorption coefficients of free **P2** (in the presence of pyridine) and complexed **P2•T2** at 750 nm (planar, ϵ_{\parallel}) and 675 nm (perpendicular, ϵ_{\perp}), after subtraction of the vibronic contribution at 675 nm in free **P2**. The vibronic contribution in liquid solution at room temperature is given by the following equation, assuming that in **P2•T2**, there is no perpendicular **P2** (i.e., all absorption at 675 nm arises from the vibronic contribution).

$$x_{vibr} = \frac{\epsilon_{675 \text{ nm}, \mathbf{T2}}}{\epsilon_{750 \text{ nm}, \mathbf{T2}}} = 0.171 \quad (2.3)$$

Thus ϵ_{\perp} can be estimated by subtracting this vibronic contribution:

$$\epsilon_{\perp, py} = x_{vibr} \times \epsilon_{675 \text{ nm}, py} = 60,960 \text{ M}^{-1} \text{ cm}^{-1} \quad (2.4)$$

Where ϵ_{py} corresponds to spectra recorded in the presence of pyridine, and $\epsilon_{\mathbf{T2}}$ to the complex **P2•T2**. Next we calculate $\Delta\epsilon_{\parallel}$. $\Delta\epsilon_{\perp}$ was found in the previous step ($60,960 \text{ M}^{-1} \text{ cm}^{-1}$) assuming all **P2** has been planarised.

$$\Delta\epsilon_{\parallel} = \epsilon_{750 \text{ nm}, \mathbf{T2}} = \epsilon_{750 \text{ nm}, py} = 103,990 \text{ M}^{-1} \text{ cm}^{-1} \quad (2.5)$$

Thus:

$$\frac{\Delta\epsilon_{||}}{\Delta\epsilon_{\perp}} = \frac{103,990}{60,960} = 1.7059 \quad (2.6)$$

Within the temperature range 298–198 K, the van't Hoff plot (Figure 2.11) of the extracted equilibrium constants shows an excellent straight-line fit, and is concentration independent across the range measured (0.8–59 μM), thus excluding the presence of aggregation. Thermodynamic parameters were extracted: $\Delta H = (5.27 \pm 0.03) \text{ kJ mol}^{-1}$ (in reasonable agreement with most computational estimates, Table 2.2), $\Delta S = (10.69 \pm 0.14) \text{ J K}^{-1} \text{ mol}^{-1}$. The large value of ΔS demonstrates an important temperature dependence for the rotational barrier: $\Delta G_{298\text{K}} = (2.08 \pm 0.05) \text{ kJ mol}^{-1}$; $\Delta G_{180\text{K}} = (3.35 \pm 0.04) \text{ kJ mol}^{-1}$ – in other words, the barrier rises as the temperature falls.

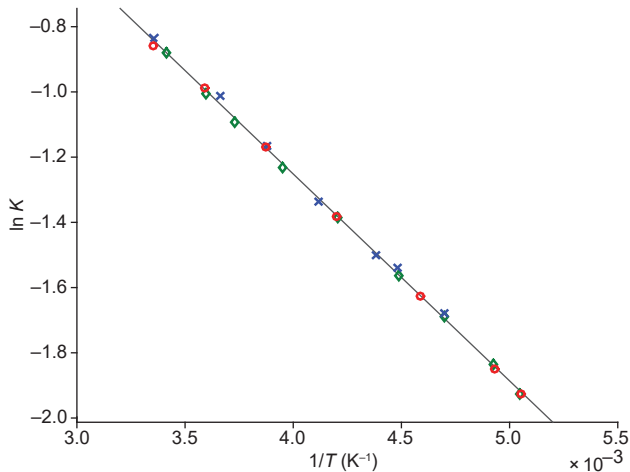


Figure 2.11: van't Hoff plot and fit line for VT experiments at three different concentrations: 0.8 μM (blue crosses), 1.6 μM (green diamonds), 58.5 μM (red circles). $R^2 = 0.999$.

There are few previous reports of the determination of both ΔH and ΔS for a torsional equilibrium. Our thermodynamic parameters for **P2** are similar to those reported for *trans-skew* isomerism in 1,1-dihalo-3-fluoro-but-1,3-dienes from solution-phase IR spectroscopy (halo = Br: $\Delta H = 3.53 \text{ kJ mol}^{-1}$, $\Delta S = 3.5 \text{ J K}^{-1} \text{ mol}^{-1}$; halo = Cl: $\Delta H = 2.95 \text{ kJ mol}^{-1}$, $\Delta S = 2.3 \text{ J K}^{-1} \text{ mol}^{-1}$).²⁰⁴ ΔS for oxalyl chloride (*trans-gauche* isomerism) has been calculated from the experimental vibrational modes (excluding the torsion mode) as $\sim 13 \text{ J K}^{-1} \text{ mol}^{-1}$,²⁰⁵ and from gas-phase electron diffraction as $10 \text{ J K}^{-1} \text{ mol}^{-1}$.²⁰⁶ We attribute our positive value of ΔS to changes in the frequencies of large-amplitude (low frequency) motions between the planar and twisted states, including the pertinent torsion mode and butadiyne bending modes.

2. Experimental and computational evaluation of the barrier to torsional rotation in a butadiyne-linked porphyrin dimer

The potential energy surface from DFT calculations (Figure 2.2) was scaled based on the experimentally determined thermodynamic parameters (ΔH and ΔS), and the Boltzmann equation (Equation 2.7) was used to determine the temperature dependence of the mole fraction of each conformer (Figure 2.12). Inclusion of the entropic factor in this manner permits a more accurate simulation of temperature-dependent populations than simply using a temperature-independent barrier height, which would overestimate conformational heterogeneity at low temperature, and underestimate it at high temperatures.

$$p_i = \frac{e^{-\frac{E_i}{k_B T}}}{\sum_{j=1}^M e^{-\frac{E_j}{k_B T}}} \quad (2.7)$$

where p_i is the population of the i^{th} state, $k_B T$ is the Boltzmann constant, and E_i is the relative energy of the i^{th} state.

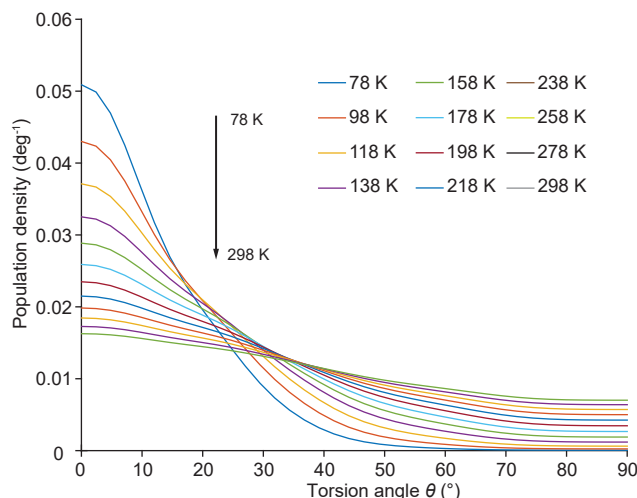


Figure 2.12: Temperature dependence of the population density for different torsion angles, based on the experimentally determined ΔH and ΔS .

The stated error in our thermodynamic parameters is the error in the fit of the experimental data to the van't Hoff equation, and must be taken in the context of the approximation of the two-state model. Our analysis presents a lower bound for the torsion barrier height, because the model evaluates the barrier between near-planar and near-perpendicular conformers. Spectral overlap between angles in a small range (estimated 0–20°) around 0° and 90° means that the absorptions at 750 nm and 675 nm capture some contributions from nearby angles.

2.4.5 Evidence for enhanced conjugation in the planar conformer from C≡C bond length and vibrational frequencies

The torsion barrier for **P2**, $\Delta H = 5.27 \text{ kJ mol}^{-1}$, can be compared to that for other alkyne- and butadiyne-linked molecules. The experimental torsion barrier of tolane ($\text{Ph}-\text{C}\equiv\text{C}-\text{Ph}$) is 2.42 kJ mol^{-1} ,²⁰⁷ compared to the near-barrierless (0.05 kJ mol^{-1}) torsion of dimethyl-acetylene ($\text{Me}\equiv\text{Me}$).²⁰⁸ Calculations have indicated that the barrier for diphenyldiacetylene (DPDA, $\text{Ph}-\text{C}\equiv\text{C}-\text{C}\equiv\text{C}-\text{Ph}$) is around 1.1 kJ mol^{-1} (PBE0/6-31+G*//6-31G* and B3LYP/6-31+G**).^{209,210}

1,4-Bis(phenylethynyl)benzene ($\text{Ph}-\text{C}\equiv\text{C}-\text{C}_6\text{H}_4-\text{C}\equiv\text{C}-\text{Ph}$) has an experimental barrier of 2.75 kJ mol^{-1} , similar to that for tolane, but DFT (B3LYP/6-31G**) dramatically overestimates the barrier at 8.75 kJ mol^{-1} .²¹¹

To ensure comparability of computational results, we have calculated the torsion barrier of tolane and DPDA at the B3LYP/6-31G* level of theory, by performing constrained geometry optimisations of planar and perpendicular conformers. At this level of theory, the barrier for DPDA is 1.1 kJ mol^{-1} , while that for tolane is 3.8 kJ mol^{-1} (calculated in this work, and in agreement with previously published data²¹²).

One might expect the torsion barrier to increase with the ability of the π -system at each end of the butadiyne to stabilise radical or anionic/cationic character, as a consequence of contributions from cumulenic resonance forms in the ground state (Figure 2.13a). Such contributions should be reflected in a decrease in the bond length alternation (BLA) in the butadiyne link (Figure 2.13b). This hypothesis is supported by our computational studies: the BLA in planar **P2** (**19d**, 0.151 \AA) is smaller than that in DPDA (0.158 \AA) as shown in Table 2.3. We used the range-separated CAM-B3LYP¹⁷⁷ functional in this part of the study: CAM-B3LYP gave BLAs in closer agreement to crystal structures than B3LYP. The more accurate estimation of BLA in polyynes when using DFT functionals with increased exact exchange (BHHLYP and CAM-B3LYP vs. B3LYP) has been reported.²¹³

The calculated BLA for perpendicular **P2** (0.163 \AA) is higher than for planar **P2** (0.151 \AA), and is even higher than both conformations of DPDA (0.158 \AA). This change in the nature of bonding between perpendicular and planar **P2** further supports the hypothesis that resonance delocalisation via a cumulenic canonical form is important in the planar conformer. The resonance stabilisation in DPDA is demonstrably lower – the calculated BLA is the same in perpendicular and planar conformers.

2. Experimental and computational evaluation of the barrier to torsional rotation in a butadiyne-linked porphyrin dimer

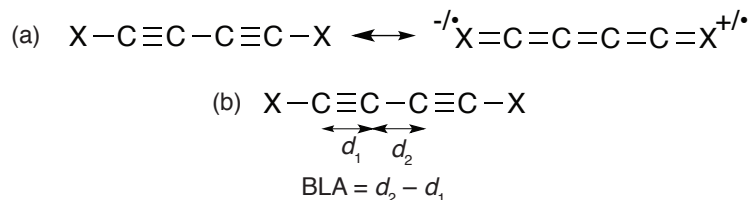


Figure 2.13: (a) A butadiyne-linked conjugated compound can be considered a combination of both alternant and cumulenic forms. The alternant form is dominant. (b) The relative contributions of these resonance structures can be estimated from the bond length alternation.

Table 2.3: Calculated and crystallographic bond length alternation (BLA) in **19d** and DPDA

Molecule	Method	Conformer	BLA(Å)
19d	CAM-B3LYP/6-31G*	$\theta = 90^\circ$	0.163
		$\theta = 0^\circ$	0.151
	crystal structure ^{168,214,215}	$\theta = 0^\circ$	0.165 ± 0.007
DPDA	CAM-B3LYP/6-31G*	$\theta = 90^\circ$	0.158
		$\theta = 0^\circ$	0.158
	crystal structure ^{216–221}	$\theta = 0^\circ$	0.178 ± 0.011

We have also compared BLA in crystal structures of **P2** vs. DPDA. We used ConQuest²²² to search the Cambridge Crystallographic Structure Database.²²³ After rejection of one DPDA structure with a high R-value (9.2%),²²⁴ we did indeed find that the mean BLA in butadiyne-linked porphyrin dimers (average of 3 structures) is less than that in unsubstituted DPDA (average of 6 structures, Table 2.3). However, the difference has low statistical significance ($p = 0.067$, Welch's t -statistic) and the sample sizes are too small to permit an unequivocal conclusion. Thus, we consider the evidence for resonance stabilisation from BLA analyses of crystal structures provisional: as more accurate crystallographic data become available, it may be possible to perform a more definitive analysis.

A contribution from cumulenic resonance forms should also be apparent in the frequency of the butadiyne $\nu_{C\equiv C}$ asymmetric stretch, observable by IR spectroscopy (2100 – 2200 cm^{−1}). We,²²⁵ and others,²²⁶ have previously used IR spectroscopy to explore cumulenic character in electronic excited states of polyynes. Increasing cumulenic character results in a lower frequency vibration. Experimentally, we see a 13 cm^{−1} difference for the $\nu_{C\equiv C}$ in experimental ATR FT-IR spectra of DPDA (2147 cm^{−1}) compared with **P2** (2134 cm^{−1}) (Table 2.4). These results are in reasonable agreement with calculation (Table 2.4). It is clear from the IR and crystallographic BLA that the contribution of cumulenic resonance structures

to the bonding in **P2** is very small, as reflected in the low barrier to torsional rotation, but that it is greater than in DPDA.

Table 2.4: Experimental and calculated acetylene stretch frequencies $\nu_{C\equiv C}$

Molecule	Method	$\nu_{C\equiv C}$ cm ⁻¹
19e (S_0)	Expt.	2134
	B3LYP/6-31G* †	2132 (2120)‡
19e (S_1)	TD-B3LYP/6-31G* †	2078 (2109)‡
DPDA	Expt.	2147
	B3LYP/6-31G* †	2156

†Planar conformer, frequencies scaled by a multiplicative factor 0.96.

‡Terminal alkyne stretch

The calculated vibrational frequencies of **P2** in its S_1 excited state show far more cumulenic character with a lower $\nu_{C\equiv C}$ (2078 cm⁻¹, Table 2.4), correlating with the increased torsion barrier (16 kJ mol⁻¹) in S_1 .³⁰ This result suggests that time-resolved IR spectroscopy could be used to probe the extent and dynamics of conjugation in the excited states of butadiyne-linked oligomers. We have previously used this technique to show cumulenic character in the first singlet and triplet excited states of a hexayne chain.²²⁵

2.4.6 Helical molecular orbitals in twisted conformers

To offer further insight into the nature of the Q-band ($S_0 \rightarrow S_1$) excitations, we have calculated the natural transition orbitals (NTOs)²²⁷ for both planar and perpendicular **P2** (Figure 2.14). The NTOs provide an intuitive picture of the natural orbital origin of the hole and electron involved in a transition. Multiple electron/hole NTO pairs may be used to describe a single transition: the relative contribution of each electron/hole pair representation to the TD-DFT transition density is denoted by an eigenvalue (λ). The NTO pair describing the $S_0 \rightarrow S_1$ (Q-band) transition in planar **P2**, ($\theta = 0^\circ$, Figure 2.14a) shows, as expected, the absence of charge transfer character in the excitation. Both hole and electron are delocalised over both porphyrin units.

Interestingly, the first two NTOs of perpendicular **P2** ($\theta = 90^\circ$, Figure 2.14b) show that this excitation can be largely described (~85%) with both hole and electron delocalised over both porphyrin units through apparent helical orbital character on the butadiyne link, arising

2. Experimental and computational evaluation of the barrier to torsional rotation in a butadiyne-linked porphyrin dimer

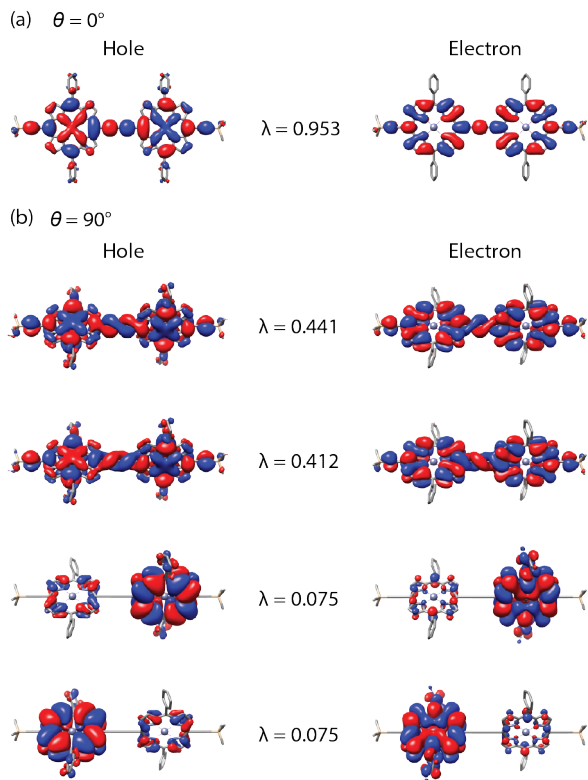


Figure 2.14: Natural transition orbitals (NTOs) calculated at the B3LYP/6-31G* level of theory for (a) planar and (b) perpendicular conformers of **19d**. The eigenvalue associated with each NTO hole/electron pair is shown as λ . The default isovalue are depicted (for $\theta = 0^\circ$, $\sim 0.01\text{\AA.u.}$; for $\theta = 90^\circ$, $\sim 0.008\text{\AA.u.}$ and $\sim 0.005\text{\AA.u.}$ for $\lambda \approx 0.4$ and $\lambda \approx 0.08$, respectively.)

from admixture of the perpendicular π_x and π_y butadiyne orbitals. The NTOs for **P2** are similar to the HOMO and LUMO for the planar and perpendicular conformers (Figure 2.15), reflecting the predominantly HOMO–LUMO nature of the $S_0 \rightarrow S_1$ transition. Helical butadiyne orbitals are also observed for the HOMO and LUMO of twisted conformers of **P2**, with increasing admixture of π_x and π_y orbitals upon twisting (Figure 2.15). Similar effects have been observed in calculations on the much simpler DPDA.²⁰⁹ The reported effects of endgroup torsion on the DFT frontier orbital energies in DPDA²⁰⁹ are similar to those reported in our previous work for **P2**.³⁰ Helical orbitals have previously been calculated by DFT for some cumulene/polyyne molecules.^{228,229} However, we are reluctant to attach much significance to the helicity in the NTOs and frontier orbitals of **P2**: the first two NTOs are pseudo-enantiomeric and near degenerate ($\lambda = 0.441$ and $\lambda = 0.412$), and their structures differ only in the phase of localised orbitals on the left hand porphyrin, and in the handedness of the helical portion of the MO. Degeneracy is broken due to the lack of symmetry in this model: the *meso*-aryl groups and terminal trimethylsilylacetylenes result

2.4. Results and discussion

in C_1 symmetry. A similar calculation performed with a truncated model (D_{2d} symmetry) gave a degenerate pair of orthogonal NTOs, with no orbital helicity (Figure 2.16). Similarly, the frontier orbitals in this symmetric model show no helical orbital character (Figure 2.17).

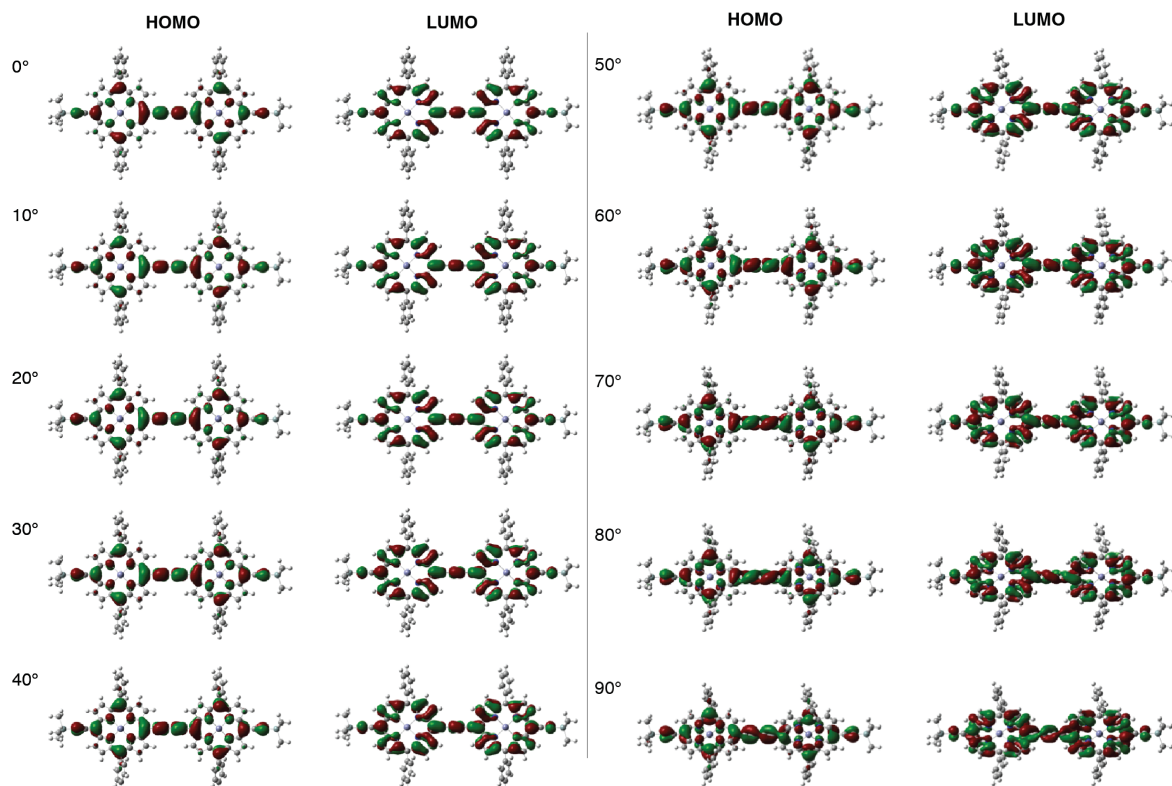


Figure 2.15: DFT (B3LYP/6-31G*/LANL2DZ) HOMO and LUMO for **P2** (model **19d**) as a function of interporphyrin torsion angle, 0–90°. The default isovalue are used, which are typically 0.08 to 0.15 Å.u.

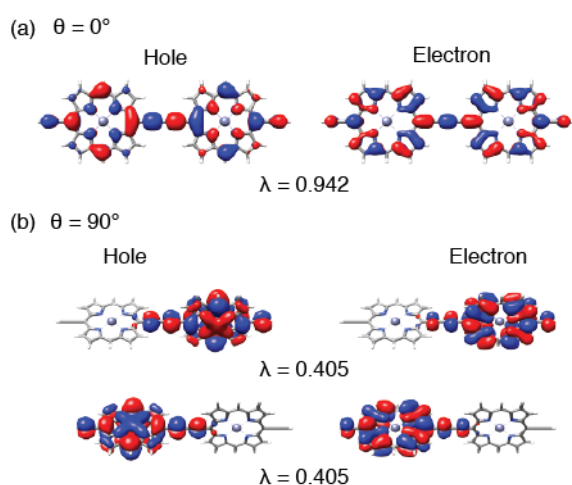


Figure 2.16: Natural transition orbitals (NTOs) for $S_0 \rightarrow S_1$ transition calculated (TD-B3LYP/6-31G*) for model **19e**. The eigenvalue associated with each NTO hole/electron pair is shown as λ . The default isovalue are used, which for all parts of the figure are $\sim 0.15 \text{ \AA.u}$.

2. Experimental and computational evaluation of the barrier to torsional rotation in a butadiyne-linked porphyrin dimer

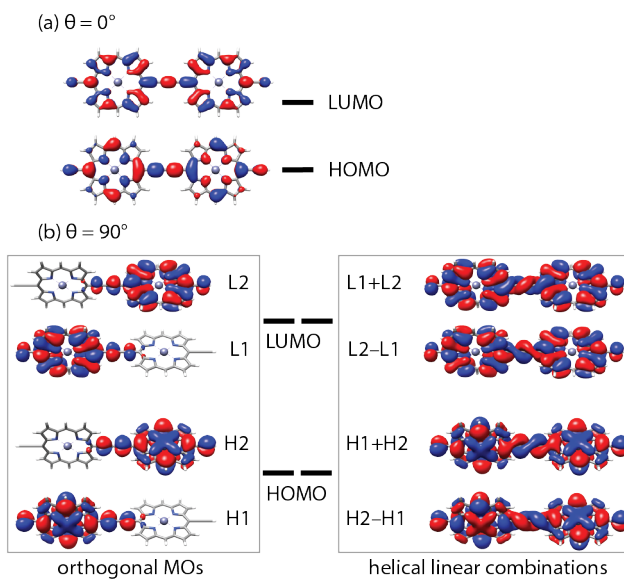


Figure 2.17: (a) Degenerate HOMO and LUMO of planar (D_{2h}) **P2** (model **19e**); (b) degenerate HOMO and LUMO of perpendicular (D_{2d}) **19e** (left) and linear combinations of the same orbitals (right), showing helical character. The default isovalue are used, which for all parts of the figure are $\sim 0.15 \text{\AA.u}$.

The equivalence of helical and localised MO representations is demonstrated by taking linear combinations of the (originally orthogonal) degenerate HOMO and LUMO of a twisted conformer (D_{2d} symmetry, B3LYP/6-31G*, Figure 2.17), giving non-orthogonal but degenerate helical orbitals. For example, in the $\theta = 90^\circ$ conformation of **19e**, there are two degenerate HOMOs, H1 and H2, each localised on one porphyrin unit; the sum and difference of these orbitals ($H1 + H2$ and $H2 - H1$) are helical, enantiomeric and degenerate. In the present study, we have found that helical orbitals occur where there is a deviation from D_{2d} symmetry (and hence frontier orbital degeneracy) in twisted conformers, either due to non-symmetric molecular structures (disordered sidegroups) or due to geometry relaxation to a minimum with a value of θ close to, but not exactly 90° .

2.5 Conclusions

The barrier to torsion about the butadiyne link in a porphyrin dimer has been determined experimentally by VT UV-Vis-NIR absorption spectroscopy. The planarisation of a twisted dimer was analysed with a van't Hoff treatment to yield the following thermodynamic parameters for planarisation: $\Delta H = (5.27 \pm 0.03) \text{ kJ mol}^{-1}$ and $\Delta S = (10.69 \pm 0.14) \text{ J K}^{-1} \text{ mol}^{-1}$.

(TD-)DFT calculations were used on model systems to explore the suitability of computational methods for the study of these chromophores. Gratifyingly, an affordable DFT

2.5. Conclusions

functional/basis set combination (B3LYP/6-31G*) provided a barrier height in reasonable agreement with experiment, and TD-DFT results permitted clear characterisation of the dimer Q-band, in agreement with previous work.³⁰ In particular, the use of TD-DFT to assign vibronic structure in the Q-band absorption was essential for the deconvolution of overlapping spectral features for the van't Hoff analysis and afforded theoretical insight into previous wavelength-selective excitation studies.

The torsion barrier in **P2** is higher than that calculated for 1,4-diphenylbutadiyne, suggesting that the increase in the size of the conjugated endcapping π -system increases the barrier height, owing to increased resonance stabilisation. Examination of the experimental $\nu_{C\equiv C}$ IR stretch and calculated BLAs offer some support to this rationale.

Appendices

References

1. M. Vicente and K. Smith, 'Syntheses and Functionalizations of Porphyrin Macrocycles', *Curr. Org. Synth.*, 2014, **11**, 3–28.
2. T. Tanaka and A. Osuka, 'Conjugated porphyrin arrays: synthesis, properties and applications for functional materials', *Chem. Soc. Rev.*, 2015, **44**, 943–969.
3. S.-P. Wang, S. Li, J. Wu, Y.-F. Shen and B.-Y. Zhu, 'Recent advances in the template-directed synthesis of porphyrin nanorings', *Chem. Comm.*, 2016, 1–14.
4. S. Hiroto, Y. Miyake and H. Shinokubo, 'Synthesis and Functionalization of Porphyrins through Organometallic Methodologies', *Chem. Rev.*, 2016, **117**, 2910–3043.
5. D. Kondratiuk, 'Synthesis and properties of giant porphyrin nanorings', Ph.D. Thesis, University of Oxford, 2013.
6. P. Liu, 'New templates for porphyrin nanorings', Ph.D. Thesis, University of Oxford, 2016.
7. N. Kamonsutthipaijit, 'Self-assembly and template-directed synthesis in multi-strand porphyrin arrays', Ph.D. Thesis, University of Oxford, 2016.
8. R. Willstätter, 'Chlorophyll', *J. Am. Chem. Soc.*, 1915, **37**, 323–345.
9. R. Robinson, 'Richard Willstatter. 1872–1942', *Obit. Not. Fellows Roy. Soc.*, 1953, **8**, 609–634.
10. A. W. Johnson, 'Aromaticity in macrocyclic polypyrrolic ring systems', *Pure Appl. Chem.*, 1971, **28**, 195–218.
11. E. Vogel, 'The porphyrins from the 'annulene chemist's' perspective', *Pure Appl. Chem.*, 1993, **65**, 143–152.
12. B. J. Littler, Y. Ciringh and J. S. Lindsey, 'Investigation of Conditions Giving Minimal Scrambling in the Synthesis of *trans*-Porphyrins from Dipyrromethanes and Aldehydes', *J. Org. Chem.*, 1999, **64**, 2864–2872.
13. B. J. Littler, M. A. Miller, C.-H. Hung, R. W. Wagner, D. F. O'Shea, P. D. Boyle and J. S. Lindsey, 'Refined Synthesis of 5-Substituted Dipyrromethanes', *J. Org. Chem.*, 1999, **64**, 1391–1396.
14. D. M. Guldin, 'Fullerene–porphyrin architectures; photosynthetic antenna and reaction center models', *Chem. Soc. Rev.*, 2002, **31**, 22–36.
15. M. Gilbert and B. Albinsson, 'Photoinduced charge and energy transfer in molecular wires', *Chem. Soc. Rev.*, 2015, **44**, 845–862.
16. S. Venkataramani, U. Jana, M. Dommaschk, F. D. Sonnichsen, F. Tuczek and R. Herges, 'Magnetic Bistability of Molecules in Homogeneous Solution at Room Temperature', *Science*, 2011, **331**, 445–448.
17. A. M. Bowen, M. W. Jones, J. E. Lovett, T. G. Gaule, M. J. McPherson, J. R. Dilworth, C. R. Timmel and J. R. Harmer, 'Exploiting orientation-selective DEER: determining molecular structure in systems containing Cu(II) centres', *Phys. Chem. Chem. Phys.*, 2016, **18**, 5981–5994.
18. D. P. Arnold, A. W. Johnson and M. Mahendran, 'Some reactions of meso-formyloctaethylporphyrin', *J. Chem. Soc., Perkin Trans. 1*, 1978, 366–370.
19. D. P. Arnold and L. J. Nitschinsk, 'Porphyrin dimers linked by conjugated butadiynes', *Tetrahedron*, 1992, **48**, 8781–8792.
20. D. P. Arnold, 'Two Rings Are Better Than One: Adventures in Porphyrin Chemistry', *Synlett*, 2000, **2000**, 296–305.

21. H. L. Anderson, 'Conjugated Porphyrin Ladders', *Inorg. Chem.*, 1994, **33**, 972–981.
22. H. L. Anderson, 'Building molecular wires from the colours of life: conjugated porphyrin oligomers', *Chem. Comm.*, 1999, 2323–2330.
23. P. N. Taylor and H. L. Anderson, 'Cooperative Self-Assembly of Double-Strand Conjugated Porphyrin Ladders', *J. Am. Chem. Soc.*, 1999, **121**, 11538–11545.
24. M. Hoffmann, J. Kärnbratt, M.-H. Chang, L. M. Herz, B. Albinsson and H. L. Anderson, 'Enhanced π conjugation around a porphyrin[6] nanoring.', *Angew. Chem. Int. Ed.*, 2008, **47**, 4993–4996.
25. M. C. O'Sullivan, J. K. Sprafke, D. V. Kondratuk, C. Rinfray, T. D. W. Claridge, A. Saywell, M. O. Blunt, J. N. O'Shea, P. H. Beton, M. Malfois and H. L. Anderson, 'Vernier templating and synthesis of a 12-porphyrin nano-ring.', *Nature*, 2011, **469**, 72–75.
26. S. A. L. Rousseaux, J. Q. Gong, R. Haver, B. Odell, T. D. W. Claridge, L. M. Herz and H. L. Anderson, 'Self-Assembly of Russian Doll Concentric Porphyrin Nanorings', *J. Am. Chem. Soc.*, 2015, **137**, 12713–12718.
27. P. Neuhaus, A. Cnossen, J. Q. Gong, L. M. Herz and H. L. Anderson, 'A Molecular Nanotube with Three-Dimensional π -Conjugation', *Angew. Chem. Int. Ed.*, 2015, **54**, 7344–7348.
28. S. J. Cole, G. C. Curthoys, E. A. Magnusson and J. N. Phillips, 'Ligand binding by metalloporphyrins. III. Thermodynamic functions for the addition of substituted pyridines to nickel(II) and zinc(II) porphyrins', *Inorg. Chem.*, 1972, **11**, 1024–1028.
29. H. J. Hogben, J. K. Sprafke, M. Hoffmann, M. Pawlicki and H. L. Anderson, 'Stepwise effective molarities in porphyrin oligomer complexes: preorganization results in exceptionally strong chelate cooperativity.', *J. Am. Chem. Soc.*, 2011, **133**, 20962–20969.
30. M. U. Winters, J. Kärnbratt, M. Eng, C. J. Wilson, H. L. Anderson and B. Albinsson, 'Photophysics of a butadiyne-linked porphyrin dimer: Influence of conformational flexibility in the ground and first singlet excited state', *J. Phys. Chem. C*, 2007, **111**, 7192–7199.
31. M. D. Peeks, P. Neuhaus and H. L. Anderson, 'Experimental and Computational Evaluation of the Barrier to Torsional Rotation in a Butadiyne-Linked Porphyrin Dimer', *Phys. Chem. Chem. Phys.*, 2016, **18**, 5264–5274.
32. R. van Grondelle, J. P. Dekker, T. Gillbro and V. Sundstrom, 'Energy transfer and trapping in photosynthesis', *Biochim. Biophys. Acta, Bioenerg.*, 1994, **1187**, 1–65.
33. G. McDermott, S. M. Prince, A. A. Freer, A. M. Hawthornthwaite-Lawless, M. Z. Papiz, R. J. Cogdell and N. W. Isaacs, 'Crystal structure of an integral membrane light-harvesting complex from photosynthetic bacteria', *Nature*, 1995, **374**, 517–521.
34. T. Higashino and H. Imahori, 'Porphyrins as excellent dyes for dye-sensitized solar cells: recent developments and insights.', *Dalton Trans.*, 2015, **44**, 448–463.
35. NREL, *Best Research Cell Efficiency*, 2016, <http://www.nrel.gov/pv/> (visited on 12/12/2016).
36. W. Shockley and H. J. Queisser, 'Detailed Balance Limit of Efficiency of p-n Junction Solar Cells', *J. Appl. Phys.*, 1961, **32**, 510–519.
37. T. D. Mody, 'Pharmaceutical development and medical applications of porphyrin-type macrocycles', *J. Porph. Phthal.*, 2000, **4**, 362–367.
38. M. Ethirajan, Y. Chen, P. Joshi and R. K. Pandey, 'The role of porphyrin chemistry in tumor imaging and photodynamic therapy.', *Chem. Soc. Rev.*, 2011, **40**, 340–362.
39. M. Stepień, N. Sprutta and L. Łatos-Grażyński, 'Figure Eights, Möbius Bands, and More: Conformation and Aromaticity of Porphyrinoids', *Angew. Chem. Int. Ed.*, 2011, **50**, 4288–4340.
40. J. Mack, 'Expanded, Contracted, and Isomeric Porphyrins: Theoretical Aspects', *Chem. Rev.*, 2016, **117**, 3444–3478.
41. E. Vogel, P. Röhrig, M. Sicken, B. Knipp, A. Herrmann, M. Pohl, H. Schmickler and J. Lex, 'The Thiophene Analogue of Porphyrin: Tetrathiaporphyrin Dication', *Angew. Chem. Int. Ed.*, 1989, **28**, 1651–1655.

References

42. E. Vogel, N. Jux, J. Dörr, T. Pelster, T. Berg, H.-S. Böhm, F. Behrens, J. Lex, D. Bremm and G. Hohlnieicher, 'Furan-Based Porphyrins: Tetraoxa[4n + 2]porphyrin Dications with 18 π -, 22 π -, or 26 π -Electron Systems', *Angew. Chem. Int. Ed.*, 2000, **39**, 1101–1105.
43. J. L. Sessler and D. Seidel, 'Synthetic Expanded Porphyrin Chemistry', *Angew. Chem. Int. Ed.*, 2003, **42**, 5134–5175.
44. S. Saito and A. Osuka, 'Expanded porphyrins: intriguing structures, electronic properties, and reactivities.', *Angew. Chem. Int. Ed.*, 2011, **50**, 4342–4373.
45. A. Osuka and S. Saito, 'Expanded porphyrins and aromaticity', *Chem. Comm.*, 2011, **47**, 4330–4339.
46. J. I. Wu, I. Fernández and P. v. R. Schleyer, 'Description of aromaticity in porphyrinoids.', *J. Am. Chem. Soc.*, 2013, **135**, 315–321.
47. M. Pawlicki and L. Latos-Grażyński, 'Aromaticity Switching in Porphyrinoids', *Chem. – Asian. J.*, 2015, **10**, 1438–1451.
48. T. Soya, W. Kim, D. Kim and A. Osuka, 'Stable [48]-, [50]-, and [52]Dodecaphyrins(1.1.0.1.1.0.1.1.0.1.1.0): The Largest Hückel Aromatic Molecules', *Chem. – Eur. J.*, 2015, **21**, 8341–8346.
49. P. v. R. Schleyer, 'Introduction: Aromaticity', *Chem. Rev.*, 2001, **101**, 1115–1118.
50. P. v. R. Schleyer, 'Introduction: Delocalization–Pi and Sigma', *Chem. Rev.*, 2005, **105**, 3433–3435.
51. N. Martín and L. T. Scott, 'Challenges in aromaticity: 150 years after Kekulé's benzene', *Chem. Soc. Rev.*, 2015, **44**, 6397–6400.
52. J.-B. Michel, Y. K. Shen, A. P. Aiden, A. Veres, M. K. Gray, J. P. Pickett, D. Hoiberg, D. Clancy, P. Norvig, J. Orwant, S. Pinker, M. A. Nowak and E. L. Aiden, 'Quantitative Analysis of Culture Using Millions of Digitized Books', *Science*, 2011, **331**, 176–182.
53. A. Kekulé, 'Ueber die Constitution und die Metamorphosen der chemischen Verbindungen und über die chemische Natur des Kohlenstoffs', *Annalen der Chemie und Pharmacie*, 1858, **106**, 129–159.
54. A. S. Couper, 'Sur une nouvelle théorie chimique', *Annales de Chimie et de Physique*, 1858, **53**, 469–489.
55. A. Kekulé, 'Sur la constitution des substances aromatiques', *Bulletin Mensuel de la Société Chimique de Paris*, 1865, **3**, 98–110.
56. A. Kekulé, 'Untersuchungen über aromatische Verbindungen Ueber die Constitution der aromatischen Verbindungen. I. Ueber die Constitution der aromatischen Verbindungen.', *Justus Liebigs Ann. Chem.*, 1866, **137**, 129–196.
57. J. Thiele, 'Zur Kenntniss der ungesättigten Verbindungen. Theorie der ungesättigten und aromatischen Verbindungen', *Justus Liebigs Ann. Chem.*, 1899, **306**, 87–142.
58. R. Willstätter and E. Waser, 'Über Cyclo-octatetraen', *Ber. Dtsch. Chem. Ges.*, 1911, **44**, 3423–3445.
59. E. C. Crocker, 'Application of the octet theory to single-ring aromatic compounds', *J. Am. Chem. Soc.*, 1922, **44**, 1618–1630.
60. J. W. Armit and R. Robinson, 'CCXI.—Polynuclear heterocyclic aromatic types. Part II. Some anhydronium bases', *J. Chem. Soc., Trans.*, 1925, **127**, 1604–1618.
61. A. T. Balaban, P. v. R. Schleyer and H. S. Rzepa, 'Crocker, Not Armit and Robinson, Begat the Six Aromatic Electrons', *Chem. Rev.*, 2005, **105**, 3436–3447.
62. L. Pauling and G. W. Wheland, 'The Nature of the Chemical Bond. V. The Quantum-Mechanical Calculation of the Resonance Energy of Benzene and Naphthalene and the Hydrocarbon Free Radicals', *J. Chem. Phys.*, 1933, **1**, 362–374.
63. E. Hückel, 'Grundzüge der Theorie ungesättigter und aromatischer Verbindungen', *Zeitschrift für Elektrochemie und angewandte physikalische Chemie*, 1937, **43**, 752–788.
64. J. Berson, *Chemical Creativity: Ideas from the Work of Woodward, Hückel, Meerwein, and Others*, Wiley, 1999.
65. W. V. E. Doering and F. L. Detert, 'Cycloheptatrienylium Oxide', *J. Am. Chem. Soc.*, 1951, **73**, 876–877.

66. A. A. Frost and B. Musulin, 'A Mnemonic Device for Molecular Orbital Energies', *J. Chem. Phys.*, 1953, **21**, 572–573.
67. T. Bally and S. Masamune, 'Cyclobutadiene', *Tetrahedron*, 1980, **36**, 343–370.
68. M. Kertesz, C. H. Choi and S. Yang, 'Conjugated polymers and aromaticity', *Chem. Rev.*, 2005, **105**, 3448–3481.
69. P. Pascal, 'Magnetochemical Researches', *Ann. Chim. Phys.*, 1910, **19**, 5–70.
70. A. Pacault, J. Hoarau and A. Marchand, in *Advances in Chemical Physics*, ed. I. Prigogine, John Wiley & Sons, Inc., 1961, vol. 3, pp. 171–238.
71. R. Gleiter and G. Haberhauer, *Aromaticity and other conjugation effects*, Wiley-VCH, Weinheim, 2012.
72. H. J. Dauben, J. D. Wilson and J. L. Laity, 'Diamagnetic Susceptibility Exaltation in Hydrocarbons', *J. Am. Chem. Soc.*, 1969, **91**, 1991–1998.
73. R. Gershoni-Poranne and A. Stanger, 'Magnetic criteria of aromaticity', *Chem. Soc. Rev.*, 2015, **44**, 6597–6615.
74. P. v. R. Schleyer and H. Jiao, 'What is aromaticity?', *Pure Appl. Chem.*, 1996, **68**, 209–218.
75. F. Sondheimer and R. Wolovsky, 'Unsaturated Macrocyclic Compounds. XXI. 1 The Synthesis of a Series of Fully Conjugated Macrocyclic Polyene-polynes (Dehydro-annulenes) from 1,5-Hexadiyne', *J. Am. Chem. Soc.*, 1962, **84**, 260–269.
76. F. Sondheimer, 'Recent advances in the chemistry of large-ring conjugated systems', *Pure Appl. Chem.*, 1963, **7**, 363–388.
77. F. Sondheimer, I. C. Calder, J. A. Elix, Y. Gaoni, P. J. Garratt, K. Grohmann, G. Di Maio, J. Mayer, M. V. Sargent and R. Wolovsky, Aromaticity, Chem. Soc. Spec. Publ. No. 21, ed. W. D. Ollis, The Chemical Society, London, 1967, pp. 75–108.
78. F. Sondheimer, 'Annulenes', *Acc. Chem. Res.*, 1972, **5**, 81–91.
79. R. Breslow, 'Aromatic Character', *Chem. Eng. News*, 1965, **43**, 90–100.
80. E. Steiner and P. W. Fowler, 'Four- and two-electron rules for diatropic and paratropic ring currents in monocyclic π -systems', *Chem. Comm.*, 2001, 2220–2221.
81. H. C. Longuet-Higgins, Aromaticity, Chem. Soc. Spec. Publ. No. 21, ed. W. D. Ollis, The Chemical Society, London, 1967, pp. 109–112.
82. J. A. Pople and K. G. Untch, 'Induced Paramagnetic Ring Currents', *J. Am. Chem. Soc.*, 1966, **88**, 4811–4815.
83. P. W. Fowler and E. Steiner, 'Patterns of Ring Currents in Conjugated Molecules: A Few-Electron Model Based on Orbital Contributions', *J. Phys. Chem. A*, 2001, **105**, 9553–9562.
84. P. Lazzaretti, 'Ring currents', *Prog. Nucl. Magn. Reson. Spectrosc.*, 2000, **36**, 1–88.
85. J. A. N. F. Gomes and R. B. Mallion, 'Aromaticity and ring currents', *Chem. Rev.*, 2001, **101**, 1349–1383.
86. E. Vogel, Aromaticity, Chem. Soc. Spec. Publ. No. 21, ed. W. D. Ollis, The Chemical Society, London, 1967, pp. 113–147.
87. J. A. Cissell, T. P. Vaid and A. L. Rheingold, 'An Antiaromatic Porphyrin Complex: Tetraphenylporphyrinato(silicon)(L)₂ (L = THF or Pyridine)', *J. Am. Chem. Soc.*, 2005, **127**, 12212–12213.
88. W. Shakespeare, *The Tragedy of Macbeth*, 1606.
89. P. v. R. Schleyer, C. Maerker, A. Dransfeld, H. Jiao and N. J. R. v. Eikema Hommes, 'Nucleus-Independent Chemical Shifts: A Simple and Efficient Aromaticity Probe', *J. Am. Chem. Soc.*, 1996, **118**, 6317–6318.
90. P. v. R. Schleyer, H. Jiao, N. J. R. v. Eikema Hommes, V. G. Malkin and O. L. Malkina, 'An Evaluation of the Aromaticity of Inorganic Rings: Refined Evidence from Magnetic Properties', *J. Am. Chem. Soc.*, 1997, **119**, 12669–12670.

References

91. S. Klod and E. Kleinpeter, 'Ab initio calculation of the anisotropy effect of multiple bonds and the ring current effect of arenes—application in conformational and configurational analysis', *J. Chem. Soc., Perkin Trans. 2*, 2001, 1893–1898.
92. R. Gershoni-Poranne and A. Stanger, 'The NICS-XY-scan: Identification of local and global ring currents in multi-ring systems', *Chem. – Eur. J.*, 2014, **20**, 5673–5688.
93. A. Stanger, 'Nucleus-independent chemical shifts (NICS): distance dependence and revised criteria for aromaticity and antiaromaticity.', *J. Org. Chem.*, 2006, **71**, 883–893.
94. Z. Chen, C. S. Wannere, C. Corminboeuf, R. Puchta and P. v. R. Schleyer, 'Nucleus-independent chemical shifts (NICS) as an aromaticity criterion', *Chem. Rev.*, 2005, **105**, 3842–3888.
95. R. Herges and D. Geuenich, 'Delocalization of Electrons in Molecules', *J. Phys. Chem. A*, 2001, **105**, 3214–3220.
96. E. U. Wallenborn, R. F. Haldimann, F. G. Klärner and F. Diederich, 'Theoretical investigation of the origin of regioselectivity in the formation of methanofullerenes by addition of diazo compounds: A model study', *Chem. – Eur. J.*, 1998, **4**, 2258–2265.
97. D. Geuenich, K. Hess, F. Köhler and R. Herges, 'Anisotropy of the induced current density (ACID), a general method to quantify and visualize electronic delocalization', *Chem. Rev.*, 2005, **105**, 3758–3772.
98. J. Jusélius, D. Sundholm and J. Gauss, 'Calculation of current densities using gauge-including atomic orbitals', *J. Chem. Phys.*, 2004, **121**, 3952–3963.
99. H. Fliegl, D. Sundholm, S. Taubert, J. Jusélius and W. Klopper, 'Magnetically induced current densities in aromatic, antiaromatic, homoaromatic, and nonaromatic hydrocarbons', *J. Phys. Chem. A*, 2009, **113**, 8668–8676.
100. H. Fliegl and D. Sundholm, 'Aromatic Pathways of Porphins, Chlorins, and Bacteriochlorins', *J. Org. Chem.*, 2012, **77**, 3408–3414.
101. J. Kruszewski and T. Krygowski, 'Definition of aromaticity basing on the harmonic oscillator model', *Tetrahedron Lett.*, 1972, **13**, 3839–3842.
102. T. M. Krygowski, M. K. Cyrański, Z. Czarnocki, G. Häfleinger and A. R. Katritzky, 'Aromaticity: A theoretical concept of immense practical importance', *Tetrahedron*, 2000, **56**, 1783–1796.
103. T. M. Krygowski and M. K. Cyrański, 'Structural Aspects of Aromaticity', *Chem. Rev.*, 2001, **101**, 1385–1420.
104. C. S. Wannere and P. v. R. Schleyer, 'How Aromatic Are Large $(4n + 2)\pi$ Annulenes?', *Org. Lett.*, 2003, **5**, 865–868.
105. C. H. Choi and M. Kertesz, 'Bond length alternation and aromaticity in large annulenes', *J. Chem. Phys.*, 1998, **108**, 6681–6688.
106. M. K. Cyrański, 'Energetic Aspects of Cyclic Pi-Electron Delocalization: Evaluation of the Methods of Estimating Aromatic Stabilization Energies', *Chem. Rev.*, 2005, **105**, 3773–3811.
107. P. v. R. Schleyer and F. Pühlhofer, 'Recommendations for the Evaluation of Aromatic Stabilization Energies', *Org. Lett.*, 2002, **4**, 2873–2876.
108. M. Mammen, E. I. Shakhnovich and G. M. Whitesides, 'Using a Convenient, Quantitative Model for Torsional Entropy To Establish Qualitative Trends for Molecular Processes That Restrict Conformational Freedom', *J. Org. Chem.*, 1998, **63**, 3168–3175.
109. F. Feixas, E. Matito, J. Poater and M. Solà, 'Quantifying aromaticity with electron delocalisation measures', *Chem. Soc. Rev.*, 2015, **44**, 6434–6451.
110. M. Palusiak and T. M. Krygowski, 'Application of AIM Parameters at Ring Critical Points for Estimation of π -Electron Delocalization in Six-Membered Aromatic and Quasi-Aromatic Rings', *Chem. – Eur. J.*, 2007, **13**, 7996–8006.
111. E. Clar, *The Aromatic Sextet*, Wiley, London, 1972.
112. M. Solà, 'Forty years of Clar's aromatic π -sextet rule', *Front. Chem.*, 2013, **1**, 4–11.

113. L. Gross, F. Mohn, N. Moll, B. Schuler, A. Criado, E. Guitian, D. Pena, A. Gourdon and G. Meyer, 'Bond-Order Discrimination by Atomic Force Microscopy', *Science*, 2012, **337**, 1326–1329.
114. J. L. von Rosenberg, J. E. Mahler and R. Pettit, 'The Bicyclo[5.1.0]Octadienyl Cation, 1A New Stable Carbonium Ion', *J. Am. Chem. Soc.*, 1962, **84**, 2842–2843.
115. F. Stahl, P. v. R. Schleyer, H. Jiao, H. F. Schaefer, K.-H. Chen and N. L. Allinger, 'Resurrection of Neutral Tris-homoaromaticity', *J. Org. Chem.*, 2002, **67**, 6599–6611.
116. E. Heilbronner, 'Hückel molecular orbitals of Möbius-type conformations of annulenes', *Tetrahedron Lett.*, 1964, **5**, 1923–1928.
117. D. Ajami, O. Oeckler, A. Simon and R. Herges, 'Synthesis of a Möbius aromatic hydrocarbon', *Nature*, 2003, **426**, 819–821.
118. P. W. Fowler and H. S. Rzepa, 'Aromaticity rules for cycles with arbitrary numbers of half-twists', *Phys. Chem. Chem. Phys.*, 2006, **8**, 1775–1777.
119. H. S. Rzepa, 'Möbius Aromaticity and Delocalization', *Chem. Rev.*, 2005, **105**, 3697–3715.
120. Z. S. Yoon, A. Osuka and D. Kim, 'Möbius aromaticity and antiaromaticity in expanded porphyrins', *Nat. Chem.*, 2009, **1**, 113–122.
121. N. C. Baird, 'Quantum organic photochemistry. II. Resonance and aromaticity in the lowest $3\pi\pi^*$ state of cyclic hydrocarbons', *J. Am. Chem. Soc.*, 1972, **94**, 4941–4948.
122. M. Rosenberg, C. Dahlstrand, K. Kilså and H. Ottosson, 'Excited state aromaticity and antiaromaticity: opportunities for photophysical and photochemical rationalizations.', *Chem. Rev.*, 2014, **114**, 5379–5425.
123. Y. M. Sung, M.-C. Yoon, J. M. Lim, H. Rath, K. Naoda, A. Osuka and D. Kim, 'Reversal of Hückel (anti)aromaticity in the lowest triplet states of hexaphyrins and spectroscopic evidence for Baird's rule', *Nat. Chem.*, 2015, **7**, 418–422.
124. J. Oh, Y. M. Sung, W. Kim, S. Mori, A. Osuka and D. Kim, 'Aromaticity reversal in the lowest excited triplet state of archetypical Möbius heteroannulenic systems', *Angew. Chem. Int. Ed.*, 2016, **55**, 6487–6491.
125. S. Taubert, D. Sundholm and F. Pichierri, 'Magnetically Induced Currents in $[n]$ Cycloparaphenylenes, $n = 6–11$ ', *J. Org. Chem.*, 2010, **75**, 5867–5874.
126. T. Kawase, 'The Synthesis and Physicochemical and Supramolecular Properties of Strained Phenylacetylene Macrocycles', *Synlett*, 2007, **2007**, 2609–2626.
127. T. J. Sisto, M. R. Golder, E. S. Hirst and R. Jasti, 'Selective Synthesis of Strained [7]Cycloparaphenylenes: An Orange-Emitting Fluorophore', *J. Am. Chem. Soc.*, 2011, **133**, 15800–15802.
128. J. Xia and R. Jasti, 'Synthesis, characterization, and crystal structure of [6]cycloparaphenylenes', *Angew. Chem. Int. Ed.*, 2012, **51**, 2474–2476.
129. N. Toriumi, A. Muranaka, E. Kayahara, S. Yamago and M. Uchiyama, 'In-Plane Aromaticity in Cycloparaphenylenes Dications: A Magnetic Circular Dichroism and Theoretical Study', *J. Am. Chem. Soc.*, 2015, **137**, 82–85.
130. A. C. Bleszynski-Jayich, W. E. Shanks, B. Peaudecerf, E. Ginossar, F. von Oppen, L. Glazman and J. G. E. Harris, 'Persistent Currents in Normal Metal Rings', *Science*, 2009, **326**, 272–275.
131. M. Mayor and C. Didschies, 'A giant conjugated molecular ring.', *Angew. Chem. Int. Ed.*, 2003, **42**, 3176–3179.
132. O. Hod, E. Rabani and R. Baer, 'Magnetoresistance of Nanoscale Molecular Devices', *Acc. Chem. Res.*, 2006, **39**, 109–117.
133. D. Rai, O. Hod and A. Nitzan, 'Magnetic Field Control of the Current through Molecular Ring Junctions', *J. Phys. Chem. Lett.*, 2011, **2**, 2118–2124.
134. A. Soncini, P. W. Fowler and L. W. Jenneskens, 'Ring currents in large $[4n + 2]$ -annulenes', *Phys. Chem. Chem. Phys.*, 2004, **6**, 277–284.

References

135. E. I. Tellgren, T. Helgaker and A. Soncini, 'Non-perturbative magnetic phenomena in closed-shell paramagnetic molecules.', *Phys. Chem. Chem. Phys.*, 2009, **11**, 5489–5498.
136. V. Chandrasekhar, R. A. Webb, M. J. Brady, M. B. Ketchen, W. J. Gallagher and A. Kleinsasser, 'Magnetic response of a single, isolated gold loop', *Phys. Rev. Lett.*, 1991, **67**, 3578–3581.
137. A. Heckmann and C. Lambert, 'Organic mixed-valence compounds: A playground for electrons and holes', *Angew. Chem. Int. Ed.*, 2012, **51**, 326–392.
138. K. Susumu, P. R. Frail, P. J. Angiolillo and M. J. Therien, 'Conjugated chromophore arrays with unusually large hole polaron delocalization lengths.', *J. Am. Chem. Soc.*, 2006, **128**, 8380–8381.
139. M. J. Therien, P. J. Angiolillo and J. Rawson, 'Extreme electron polaron spatial delocalization in π -conjugated materials', *Proc. Natl. Acad. Sci. USA*, 2015, **112**, 13779–13783.
140. N. Takeda, S. Asaoka and J. R. Miller, 'Nature and Energies of Electrons and Holes in a Conjugated Polymer, Polyfluorene', *J. Am. Chem. Soc.*, 2006, **128**, 16073–16082.
141. L. Zaikowski, P. Kaur, C. Gelfond, E. Selvaggio, S. Asaoka, Q. Wu, H.-C. Chen, N. Takeda, A. R. Cook, A. Yang, J. Rosanelli and J. R. Miller, 'Polarons, Bipolarons, and Side-By-Side Polarons in Reduction of Oligofluorenes', *J. Am. Chem. Soc.*, 2012, **134**, 10852–10863.
142. J. Bakalis, A. R. Cook, S. Asaoka, M. Forster, U. Scherf and J. R. Miller, 'Polarons, compressed polarons, and bipolarons in conjugated polymers', *J. Phys. Chem. C*, 2014, **118**, 114–125.
143. N. Takeda and J. R. Miller, 'Poly(3-decythiophene) Radical Anions and Cations in Solution: Single and Multiple Polarons and Their Delocalization Lengths in Conjugated Polymers', *J. Phys. Chem. B*, 2012, **116**, 14715–14723.
144. T. D. Nguyen, G. Hukic-Markosian, F. Wang, L. Wojcik, X.-G. Li, E. Ehrenfreund and Z. V. Vardeny, 'Isotope effect in spin response of π -conjugated polymer films and devices.', *Nat. Mater.*, 2010, **9**, 345–352.
145. F. C. Grozema, P. T. van Duijnen, Y. A. Berlin, M. A. Ratner and L. D. A. Siebbeles, 'Intramolecular Charge Transport along Isolated Chains of Conjugated Polymers: Effect of Torsional Disorder and Polymerization Defects', *J. Phys. Chem. B*, 2002, **106**, 7791–7795.
146. J. Roncali, 'Synthetic Principles for Bandgap Control in Linear π -Conjugated Systems', *Chem. Rev.*, 1997, **97**, 173–206.
147. A. Pron, P. Gawrys, M. Zagorska, D. Djurado and R. Demadrille, 'Electroactive materials for organic electronics: preparation strategies, structural aspects and characterization techniques', *Chem. Soc. Rev.*, 2010, **39**, 2577–2632.
148. J. M. Tour, 'Molecular electronics. Synthesis and testing of components', *Acc. Chem. Res.*, 2000, **33**, 791–804.
149. R. L. Carroll and C. B. Gorman, 'The genesis of molecular electronics', *Angew. Chem. Int. Ed.*, 2002, **41**, 4378–4400.
150. N. Robertson and C. A. McGowan, 'A comparison of potential molecular wires as components for molecular electronics.', *Chem. Soc. Rev.*, 2003, **32**, 96–103.
151. R. M. Metzger, 'Unimolecular Electronics', *Chem. Rev.*, 2015, **115**, 5056–5115.
152. R. E. Martin and F. Diederich, 'Linear Monodisperse π -Conjugated Oligomers: Model Compounds for Polymers and More', *Angew. Chem. Int. Ed.*, 1999, **38**, 1350–1377.
153. W. B. Davis, M. A. Ratner and M. R. Wasielewski, 'Conformational gating of long distance electron transfer through wire-like bridges in donor-bridge-acceptor molecules', *J. Am. Chem. Soc.*, 2001, **123**, 7877–7886.
154. N. Yoshida, T. Ishizuka, A. Osuka, D. H. Jeong, H. S. Cho, D. Kim, Y. Matsuzaki, A. Nogami and K. Tanaka, 'Fine Tuning of Photophysical Properties of meso–meso-Linked Zn^{II}-Diporphyrins by Dihedral Angle Control', *Chem. – Eur. J.*, 2003, **9**, 58–75.
155. L. Venkataraman, J. E. Klare, C. Nuckolls, M. S. Hybertsen and M. L. Steigerwald, 'Dependence of single-molecule junction conductance on molecular conformation.', *Nature*, 2006, **442**, 904–907.

156. T. K. Ahn, K. S. Kim, D. Y. Kim, S. B. Noh, N. Aratani, C. Ikeda, A. Osuka and D. Kim, 'Relationship between Two-Photon Absorption and the π -Conjugation Pathway in Porphyrin Arrays through Dihedral Angle Control', *J. Am. Chem. Soc.*, 2006, **128**, 1700–1704.
157. M.-H. Chang, M. Hoffmann, H. L. Anderson and L. M. Herz, 'Dynamics of excited-state conformational relaxation and electronic delocalization in conjugated porphyrin oligomers.', *J. Am. Chem. Soc.*, 2008, **130**, 10171–10178.
158. A. A. Kocherzhenko, K. B. Whaley, G. Sforazzini, H. L. Anderson, M. Wykes, D. Beljonne, F. C. Grozema and L. D. A. Siebbeles, 'Effects of the Environment on Charge Transport in Molecular Wires', *J. Phys. Chem. C*, 2012, **116**, 25213–25225.
159. L. Sun, Y. A. Diaz-Fernandez, T. A. Gschneidtner, F. Westerlund, S. Lara-Avila and K. Moth-Poulsen, 'Single-molecule electronics: from chemical design to functional devices.', *Chem. Soc. Rev.*, 2014, **43**, 7378–7411.
160. V. S.-Y. Lin, S. G. DiMagno and M. J. Therien, 'Highly Conjugated, Acetylenyl Bridged Porphyrins: New Models for Light-Harvesting Antenna Systems', *Science*, 1994, **264**, 1105–1111.
161. V. S.-Y. Lin and M. J. Therien, 'The Role of Porphyrin-to-Porphyrin Linkage Topology in the Extensive Modulation of the Absorptive and Emissive Properties of a Series of Ethynyl- and Butadiynyl-Bridged Bis- and Tris(porphinato)zinc Chromophores', *Chem. – Eur. J.*, 1995, **1**, 645–651.
162. H. A. Collins, M. Khurana, E. H. Moriyama, A. Mariampillai, E. Dahlstedt, M. Balaz, M. K. Kuimova, M. Drobizhev, V. X. D. Yang, D. Phillips, A. Rebane, B. C. Wilson and H. L. Anderson, 'Blood-vessel closure using photosensitizers engineered for two-photon excitation', *Nat. Photon.*, 2008, **2**, 420–424.
163. J. D. Wilkinson, G. Wicks, A. Nowak-Król, Ł. G. Łukasiewicz, C. J. Wilson, M. Drobizhev, A. Rebane, D. T. Gryko and H. L. Anderson, 'Two-photon absorption in butadiyne-linked porphyrin dimers: torsional and substituent effects', *J. Mat. Chem. C*, 2014, **2**, 6802–6809.
164. Y. Nakamura, N. Aratani and A. Osuka, 'Cyclic porphyrin arrays as artificial photosynthetic antenna: synthesis and excitation energy transfer.', *Chem. Soc. Rev.*, 2007, **36**, 831–845.
165. G. Sedghi, K. Sawada, L. J. Esdaile, M. Hoffmann, H. L. Anderson, D. Bethell, W. Haiss, S. J. Higgins and R. J. Nichols, 'Single Molecule Conductance of Porphyrin Wires with Ultralow Attenuation', *J. Am. Chem. Soc.*, 2008, **130**, 8582–8583.
166. G. Sedghi, V. M. García-Suárez, L. J. Esdaile, H. L. Anderson, C. J. Lambert, S. Martín, D. Bethell, S. J. Higgins, M. Elliott, N. Bennett, J. E. Macdonald and R. J. Nichols, 'Long-range electron tunnelling in oligo-porphyrin molecular wires', *Nat. Nanotech.*, 2011, **6**, 517–523.
167. G. Sedghi, L. J. Esdaile, H. L. Anderson, S. Martin, D. Bethell, S. J. Higgins and R. J. Nichols, 'Comparison of the conductance of three types of porphyrin-based molecular wires: β -meso, β -fused tapes, meso-butadiyne-linked and twisted meso-meso linked oligomers', *Adv. Mat.*, 2012, **24**, 653–657.
168. P. N. Taylor, J. Huuskonen, G. Rumbles, R. T. Aplin, E. Williams and H. L. Anderson, 'Conjugated porphyrin oligomers from monomer to hexamer', *Chem. Comm.*, 1998, 909–910.
169. M. Hoffmann, C. J. Wilson, B. Odell and H. L. Anderson, 'Template-directed synthesis of a π -conjugated porphyrin nanoring.', *Angew. Chem. Int. Ed.*, 2007, **46**, 3122–3125.
170. J. K. Sprafke, B. Odell, T. D. W. Claridge and H. L. Anderson, 'All-or-nothing cooperative self-assembly of an annulene sandwich', *Angew. Chem. Int. Ed.*, 2011, **50**, 5572–5575.
171. M. J. Frampton, H. Akdas, A. R. Cowley, J. E. Rogers, J. E. Slagle, P. A. Fleitz, M. Drobizhev, A. Rebane and H. L. Anderson, 'Synthesis, Crystal Structure, and Nonlinear Optical Behavior of β -Unsubstituted meso–meso E-Vinylene-Linked Porphyrin Dimers', *Org. Lett.*, 2005, **7**, 5365–5368.
172. J. S. Lindsey, S. Prathapan, T. E. Johnson and R. W. Wagner, 'Porphyrin building blocks for modular construction of bioorganic model systems', *Tetrahedron*, 1994, **50**, 8941–8968.
173. R. W. Wagner, T. E. Johnson, F. Li and J. S. Lindsey, 'Synthesis of Ethyne-Linked or Butadiyne-Linked Porphyrin Arrays Using Mild, Copper-Free, Pd-Mediated Coupling Reactions', *J. Org. Chem.*, 1995, **60**, 5266–5273.

References

174. M. Pawlicki, M. Morisue, N. K. S. Davis, D. G. McLean, J. E. Haley, E. Beuerman, M. Drobizhev, A. Rebane, A. L. Thompson, S. I. Pascu, G. Accorsi, N. Armaroli and H. L. Anderson, 'Engineering conjugation in para-phenylene-bridged porphyrin tapes', *Chem. Sci.*, 2012, **3**, 1541–1547.
175. A. Tsuda, H. Furuta and A. Osuka, 'Syntheses, structural characterizations, and optical and electrochemical properties of directly fused diporphyrins.', *J. Am. Chem. Soc.*, 2001, **123**, 10304–10321.
176. R. Stranger, J. E. McGrady, D. P. Arnold, I. Lane and G. A. Heath, 'Communication between Porphyrin Rings in the Butadiyne-Bridged Dimer Ni(OEP)(μ -C₄)Ni(OEP): A Density Functional Study', *Inorg. Chem.*, 1996, **35**, 7791–7797.
177. T. Yanai, D. P. Tew and N. C. Handy, 'A new hybrid exchange-correlation functional using the Coulomb-attenuating method (CAM-B3LYP)', *Chem. Phys. Lett.*, 2004, **393**, 51–57.
178. L. Rintoul, S. R. Harper and D. P. Arnold, 'A systematic theoretical study of the electronic structures of porphyrin dimers: DFT and TD-DFT calculations on diporphyrins linked by ethane, ethene, ethyne, imine, and azo bridges.', *Phys. Chem. Chem. Phys.*, 2013, **15**, 18951–18964.
179. M. K. Kuimova, M. Balaz, H. L. Anderson and P. R. Ogilby, 'Intramolecular rotation in a porphyrin dimer controls singlet oxygen production.', *J. Am. Chem. Soc.*, 2009, **131**, 7948–7949.
180. M. K. Kuimova, S. W. Botchway, A. W. Parker, M. Balaz, H. A. Collins, H. L. Anderson, K. Suhling and P. R. Ogilby, 'Imaging intracellular viscosity of a single cell during photoinduced cell death.', *Nat. Chem.*, 2009, **1**, 69–73.
181. A. Vyniauskas, M. Qurashi, N. Gallop, M. Balaz, H. L. Anderson and M. K. Kuimova, 'Unravelling the effect of temperature on viscosity-sensitive fluorescent molecular rotors', *Chem. Sci.*, 2015, **6**, 5773–5778.
182. M. Drobizhev, Y. Stepanenko, A. Rebane, C. J. Wilson, T. E. Screen and H. L. Anderson, 'Strong cooperative enhancement of two-photon absorption in double-strand conjugated porphyrin ladder arrays', *J. Am. Chem. Soc.*, 2006, **128**, 12432–12433.
183. F. C. Grozema, C. Houarner-Rassin, P. Prins, L. D. A. Siebbeles and H. L. Anderson, 'Supramolecular control of charge transport in molecular wires.', *J. Am. Chem. Soc.*, 2007, **129**, 13370–13371.
184. M. U. Winters, J. Kärnbratt, H. E. Blades, C. J. Wilson, M. J. Frampton, H. L. Anderson and B. Albinsson, 'Control of electron transfer in a conjugated porphyrin dimer by selective excitation of planar and perpendicular conformers', *Chem. – Eur. J.*, 2007, **13**, 7385–7394.
185. A. Tsuda, H. Hu, R. Tanaka and T. Aida, 'Planar or perpendicular? Conformational preferences of π -conjugated metalloporphyrin dimers and trimers in supramolecular tubular arrays', *Angew. Chem. Int. Ed.*, 2005, **44**, 4884–4888.
186. C. E. Tait, P. Neuhaus, M. D. Peeks, H. L. Anderson and C. R. Timmel, 'Transient EPR Reveals Triplet State Delocalization in a Series of Cyclic and Linear π -Conjugated Porphyrin Oligomers', *J. Am. Chem. Soc.*, 2015, **137**, 8284–8293.
187. M. J. Frisch, G. W. Trucks, H. B. Schlegel, G. E. Scuseria, M. A. Robb, J. R. Cheeseman, G. Scalmani, V. Barone, B. Mennucci, G. A. Petersson, H. Nakatsuji, M. Caricato, X. Li, H. P. Hratchian, A. F. Izmaylov, J. Bloino, G. Zheng, J. L. Sonnenberg, M. Hada, M. Ehara, K. Toyota, R. Fukuda, J. Hasegawa, M. Ishida, T. Nakajima, Y. Honda, O. Kitao, H. Nakai, T. Vreven, J. A. Montgomery Jr., J. E. Peralta, F. Ogliaro, M. Bearpark, J. J. Heyd, E. Brothers, K. N. Kudin, V. N. Staroverov, R. Kobayashi, J. Normand, K. Raghavachari, A. Rendell, J. C. Burant, S. S. Iyengar, J. Tomasi, M. Cossi, N. Rega, J. M. Millam, M. Klene, J. E. Knox, J. B. Cross, V. Bakken, C. Adamo, J. Jaramillo, R. Gomperts, R. E. Stratmann, O. Yazyev, A. J. Austin, R. Cammi, C. Pomelli, J. W. Ochterski, R. L. Martin, K. Morokuma, V. G. Zakrzewski, G. A. Voth, P. Salvador, J. J. Dannenberg, S. Dapprich, A. D. Daniels, Ö. Farkas, J. B. Foresman, J. V. Ortiz, J. Cioslowski and D. J. Fox, *Gaussian 09 Revision D.01*, software, Wallingford CT, 2009.
188. A. D. Becke, 'Density-functional thermochemistry. III. The role of exact exchange', *J. Chem. Phys.*, 1993, **98**, 5648–5652.

189. R. Ditchfield, W. J. Hehre and J. A. Pople, 'Self-Consistent Molecular-Orbital Methods. IX. An Extended Gaussian-Type Basis for Molecular-Orbital Studies of Organic Molecules', *J. Chem. Phys.*, 1971, **54**, 724–728.
190. W. J. Hehre, R. Ditchfield and J. A. Pople, 'Self-Consistent Molecular Orbital Methods. XII. Further Extensions of Gaussian-Type Basis Sets for Use in Molecular Orbital Studies of Organic Molecules', *J. Chem. Phys.*, 1972, **56**, 2257–2261.
191. P. C. Hariharan and J. A. Pople, 'The influence of polarization functions on molecular orbital hydrogenation energies', *Theor. Chim. Acta*, 1973, **28**, 213–222.
192. V. A. Rassolov, J. A. Pople, M. A. Ratner and T. L. Windus, '6-31G* basis set for atoms K through Zn', *J. Chem. Phys.*, 1998, **109**, 1223–1229.
193. P. J. Hay and W. R. Wadt, 'Ab initio effective core potentials for molecular calculations. Potentials for the transition metal atoms Sc to Hg', *J. Chem. Phys.*, 1985, **82**, 270–283.
194. P. J. Hay and W. R. Wadt, 'Ab initio effective core potentials for molecular calculations. Potentials for K to Au including the outermost core orbitals', *J. Chem. Phys.*, 1985, **82**, 299–310.
195. E. F. Pettersen, T. D. Goddard, C. C. Huang, G. S. Couch, D. M. Greenblatt, E. C. Meng and T. E. Ferrin, 'UCSF Chimera—a visualization system for exploratory research and analysis', *J. Comp. Chem.*, 2004, **25**, 1605–1612.
196. G. U. Bublitz and S. G. Boxer, 'Effective polarity of frozen solvent glasses in the vicinity of dipolar solutes', *J. Am. Chem. Soc.*, 1998, **120**, 3988–3992.
197. J. Kärnbratt, M. Gilbert, J. K. Sprafke, H. L. Anderson and B. Albinsson, 'Self-Assembly of Linear Porphyrin Oligomers into Well-Defined Aggregates', *J. Phys. Chem. C*, 2012, **116**, 19630–19635.
198. M. Hutin, J. K. Sprafke, B. Odell, H. L. Anderson and T. D. Claridge, 'A discrete three-layer stack aggregate of a linear porphyrin tetramer: solution-phase structure elucidation by NMR and X-ray scattering', *J. Am. Chem. Soc.*, 2013, **135**, 12798–12807.
199. H. L. Anderson, 'Supramolecular orientation of conjugated porphyrin oligomers in stretched polymers', *Adv. Mat.*, 1994, **6**, 834–836.
200. M. Drobizhev, Y. Stepanenko, Y. Dzenis, A. Karotki, A. Rebane, P. N. Taylor and H. L. Anderson, 'Extremely Strong Near-IR Two-Photon Absorption in Conjugated Porphyrin Dimers: Quantitative Description with Three-Essential-States Model', *J. Phys. Chem. B*, 2005, **109**, 7223–7236.
201. F. Santoro, A. Lami, R. Improta, J. Bloino and V. Barone, 'Effective method for the computation of optical spectra of large molecules at finite temperature including the Duschinsky and Herzberg-Teller effect: the Q_x band of porphyrin as a case study.', *J. Chem. Phys.*, 2008, **128**, 224311–224317.
202. V. Barone, J. Bloino, M. Biczysko and F. Santoro, 'Fully Integrated Approach to Compute vibrationally Resolved Optical Spectra: From Small Molecules to Macrosystems', *J. Chem. Theory Comput.*, 2009, **5**, 540–554.
203. F. V. A. Camargo, H. L. Anderson, S. R. Meech and I. A. Heisler, 'Full Characterization of Vibrational Coherence in a Porphyrin Chromophore by Two-Dimensional Electronic Spectroscopy', *J. Phys. Chem. A*, 2015, **119**, 95–101.
204. K. O. Hartman, G. L. Carlson, R. E. Witkowski and W. G. Fateley, 'The measurement of conformational equilibria via the infrared studies of 1,1-dibromo-3-fluorobutadiene-1,3 and 1,1-dichloro-3-fluorobutadiene-1,3', *Spectrochim. Acta Mol. Biomol. Spectrosc.*, 1968, **24**, 157–167.
205. J. R. Durig, J. Liu, T. S. Little and V. F. Kalasinsky, 'Conformational analysis, barriers to internal rotation, vibrational assignment, and ab initio calculations of 1,2-difluoroethane', *J. Phys. Chem.*, 1992, **96**, 8224–8233.
206. K. Hagen and K. Hedberg, 'Conformational analysis. I. Molecular structure, composition, trans-gauche energy and entropy differences, and potential hindering internal rotation of gaseous oxaly chloride as determined by electron diffraction', *J. Am. Chem. Soc.*, 1973, **95**, 1003–1009.
207. K. Okuyama, T. Hasegawa, M. Ito and N. Mikami, 'Electronic spectra of tolan in a supersonic free jet: large-amplitude torsional motion', *J. Phys. Chem.*, 1984, **88**, 1711–1716.

References

208. W. Olson and D. Papousek, 'High-resolution infrared spectra of ethanelike molecules and the barrier to internal rotation: The ν_9 , ν_{13} band of dimethylacetylene', *J. Mol. Spectrosc.*, 1971, **37**, 527–534.
209. P. W. Thulstrup, S. V. Hoffmann, B. K. V. Hansen and J. Spanget-Larsen, 'Unique interplay between electronic states and dihedral angle for the molecular rotor diphenyldiacetylene.', *Phys. Chem. Chem. Phys.*, 2011, **13**, 16168–16174.
210. J. A. Sebree and T. S. Zwier, 'The excited states and vibronic spectroscopy of diphenyldiacetylene and diphenylvinylacetylene', *Phys. Chem. Chem. Phys.*, 2012, **14**, 173–183.
211. S. J. Greaves, E. L. Flynn, E. L. Futcher, E. Wrede, D. P. Lydon, P. J. Low, S. R. Rutter and A. Beeby, 'Cavity ring-down spectroscopy of the torsional motions of 1,4-bis(phenylethyynyl)benzene', *J. Phys. Chem. A*, 2006, **110**, 2114–2121.
212. M. Wierzbicka, I. Byliska, C. Czaplewski and W. Wiczk, 'Experimental and theoretical studies of the spectroscopic properties of simple symmetrically substituted diphenylacetylene derivatives', *RSC Adv.*, 2015, **5**, 29294–29303.
213. M. J. G. Peach, E. I. Tellgren, P. Saek, T. Helgaker and D. J. Tozer, 'Structural and electronic properties of polyacetylene and polyyne from hybrid and Coulomb-attenuated density functionals', *J. Phys. Chem. A*, 2007, **111**, 11930–11935.
214. A. Berlicka, L. Latos-Grazyski and T. Lis, '1H NMR investigation of high-spin and low-spin iron(III) meso-ethynylporphyrins', *Inorg. Chem.*, 2005, **44**, 4522–4533.
215. Y.-J. Chen, S.-S. Chen, S.-S. Lo, T.-H. Huang, C.-C. Wu, G.-H. Lee, S.-M. Peng and C.-Y. Yeh, 'Porphyrin dimers bridged by a platinumdiacetylidyne unit', *Chem. Comm.*, 2006, **5**, 1015–1017.
216. G. W. Coates, A. R. Dunn, L. M. Henling, D. A. Dougherty and R. H. Grubbs, 'Phenyl–Perfluorophenyl Stacking Interactions: A New Strategy for Supermolecule Construction', *Angew. Chem. Int. Ed.*, 1997, **36**, 248–251.
217. C. Glock, F. M. Younis, S. Ziemann, H. Görls, W. Imhof, S. Krieck and M. Westerhausen, '2,6-Diisopropylphenylamides of Potassium and Calcium: A Primary Amido Ligand in s-Block Metal Chemistry with an Unprecedented Catalytic Reactivity', *Organometallics*, 2013, **32**, 2649–2660.
218. M. Gdaniec, W. Jankowski, M. J. Milewska and T. Pooński, 'Supramolecular Assemblies of Hydrogen-Bonded Carboxylic Acid Dimers Mediated by PhenylPentafluorophenyl Stacking Interactions', *Angew. Chem. Int. Ed.*, 2003, **42**, 3903–3906.
219. J. K. D. Surette, M.-A. MacDonald, M. J. Zaworotko and R. D. Singer, 'X-ray crystal structure of 1,4-diphenylbutadiyne', *J. Chem. Crystallogr.*, 1994, **24**, 715–717.
220. F. R. Fronczek and M. S. Erickson, 'Refinements of the crystal structures of 1,4-diphenylbutadiyne and its complex with two moles of $\text{Co}_2(\text{CO})_6$ ', *J. Chem. Crystallogr.*, 1995, **25**, 737–742.
221. M. Shi and H.-X. Qian, 'NHC Pd(II) complex Cu(I) co-catalyzed homocoupling reaction of terminal alkynes', *Appl. Organomet. Chem.*, 2006, **20**, 771–774.
222. I. J. Bruno, J. C. Cole, P. R. Edgington, M. Kessler, C. F. Macrae, P. McCabe, J. Pearson and R. Taylor, 'New software for searching the Cambridge Structural Database and visualizing crystal structures.', *Acta Crystallogr., Sect. B: Struct. Sci., Cryst. Eng. Mater.*, 2002, **58**, 389–397.
223. F. H. Allen, 'The Cambridge Structural Database: a quarter of a million crystal structures and rising.', *Acta Crystallogr., Sect. B: Struct. Sci., Cryst. Eng. Mater.*, 2002, **58**, 380–388.
224. R. Thomas, S. S. Mallajyosula, S. Lakshmi, S. K. Pati and G. Kulkarni, 'Conjugation in 1,4-diphenylbutadiyne and 1,2-diphenylacetylene: A combined experimental and theoretical study', *J. Mol. Struct.*, 2009, **922**, 46–50.
225. L. D. Movsisyan, M. D. Peeks, G. M. Greetham, M. Towrie, A. L. Thompson, A. W. Parker and H. L. Anderson, 'Photophysics of Threaded sp-Carbon Chains: The Polyyne is a Sink for Singlet and Triplet Excitation', *J. Am. Chem. Soc.*, 2014, **136**, 17996–18008.
226. M. M. Yildizhan, D. Fazzi, A. Milani, L. Brambilla, M. Del Zoppo, W. A. Chalifoux, R. R. Tykwiński and G. Zerbi, 'Photogenerated cumulenic structure of adamantyl endcapped linear carbon chains: an experimental and computational investigation based on infrared spectroscopy.', *J. Chem. Phys.*, 2011, **134**, 124512.

References

227. R. L. Martin, 'Natural transition orbitals', *J. Chem. Phys.*, 2003, **118**, 4775–4777.
228. C. H. Hendon, D. Tiana, A. T. Murray, D. R. Carbery and A. Walsh, 'Helical frontier orbitals of conjugated linear molecules', *Chem. Sci.*, 2013, **4**, 4278–4284.
229. M. Liu, V. I. Artyukhov, H. Lee, F. Xu and B. I. Yakobson, 'Carbyne from First Principles: Chain of C Atoms, a Nanorod or a Nanorope', *ACS Nano*, 2013, **7**, 10075–10082.